

1 Proposal for a Full-Scale Detector Engineering Test
2 and Test Beam Calibration of a Single-Phase LAr
3 TPC

4 A. name1¹, B. name2², and C. name3³

5 ¹Department of X1, University Y1

6 ²Department of X2, University Y2

7 ³Department of X3, University YY3

8 March 17, 2015

9 **Abstract**

10 After a short introduction to the ELBNF physics program we motivate the pro-
11 posed single phase liquid argon detector and charged particle beam measurement
12 program. We describe the required beam line and beam monitoring instrumen-
13 tation for the project. The proposed single phase liquid argon detector presently
14 described corresponds to the LBNE detector design. Discussions about alternate
15 designs are in progress and this proposal will be updated according to a developing
16 consensus on the detector design. The detector will be placed inside a membrane
17 cryostat which will be connected to a cryogenics systems for which we provide
18 engineering details. The proposal concludes with a description of data handling
19 and analysis plans, as well as a schedule and an overview of the organizational
20 structure put in place to execute the plan.

21 Contents

| | | |
|----|--|----|
| 22 | 1 Introduction [~5 pages; Thomas/Greg/B.Wilson] | 3 |
| 23 | 1.1 Key physics goals of ELBNF | 4 |
| 24 | 1.2 Single-phase LAr detector | 4 |
| 25 | 1.3 Goals for the prototype detector and beam test | 5 |
| 26 | 2 CERN prototype detector and charged particle beam test [~10 pages; Donna/Jarek] | 6 |
| 28 | 2.1 Requirements for the detector, beam and commissioning | 7 |
| 29 | 2.2 Detector performance tests | 11 |
| 30 | 2.3 Other measurements | 13 |
| 31 | 3 Single Phase LAr Detector [~10 pages; J. Stewart et al.] | 13 |
| 32 | 3.1 ELBNF detector | 13 |
| 33 | 3.2 CERN prototype detector | 15 |
| 34 | 4 Cryostat and cryogenics system [~5 pages; David/Barry/Jack] | 29 |
| 35 | 4.1 Cryostat | 29 |
| 36 | 4.2 Cryostat size from TPC dimensions (Move to begining of sec 4 per DM) | 38 |
| 37 | 4.3 Cryogenic System | 39 |
| 38 | 5 Charged Particle Test Beam Requirements [~10 pages; Cheng-Ju] | 41 |
| 39 | 5.1 Particle Beam Requirements | 41 |
| 40 | 5.2 EHN1 H4ext Beamlne | 42 |
| 41 | 5.3 Beam Instrumentation | 43 |
| 42 | 5.4 Beam Window on LAr Cryostat | 44 |
| 43 | 6 Computing requirements, data handling and software [~3 pages; Maxim/Craig] | 45 |
| 44 | 6.1 Collecting and Storing Raw Data | 45 |
| 45 | 6.2 Databases | 48 |
| 46 | 6.3 A note on Simulation and Reconstruction Software | 48 |
| 47 | 6.4 Distributed Computing, Workload and Workflow Management | 48 |
| 48 | 7 CERN neutrino platform test environment [5 pages; David/Jack/Cheng-Ju/Thomas] | 50 |
| 49 | | 50 |
| 50 | 8 Schedule, organization and cost estimate [~5 pages; Thomas/Greg] | 50 |
| 51 | 8.1 Schedule | 50 |
| 52 | 8.2 Organization | 51 |
| 53 | 8.3 Division of Responsibilities | 51 |
| 54 | 9 Summary [~2 pages; Thomas/Greg] | 52 |

55 1 Introduction [~5 pages; Thomas/Greg/B.Wilson]

56 The preponderance of matter over antimatter in the early Universe, the dynamics of
57 the supernova bursts that produced the heavy elements necessary for life and whether
58 protons eventually decay - these mysteries at the forefront of particle physics and astro-
59 physics are key to understanding the early evolution of our Universe, its current state
60 and its eventual fate. The Experiment at the Long-Baseline Neutrino Facility (ELBNF)
61 represents an extensively developed plan for a world-class experiment dedicated to ad-
62 dressing these questions.

63 Experiments carried out over the past half century have revealed that neutrinos
64 are found in three states, or flavors, and can transform from one flavor into another.
65 These results indicate that each neutrino flavor state is a mixture of three different
66 nonzero mass states, and to date offer the most compelling evidence for physics beyond
67 the Standard Model. In a single experiment, ELBNF will enable a broad exploration
68 of the three-flavor model of neutrino physics with unprecedented detail. Chief among
69 its potential discoveries is that of matter-antimatter asymmetries (through the mech-
70 anism of charge-parity violation) in neutrino flavor mixing - a step toward unraveling
71 the mystery of matter generation in the early Universe. Independently, determination
72 of the unknown neutrino mass ordering and precise measurement of neutrino mixing
73 parameters by ELBNF may reveal new fundamental symmetries of Nature.

74 Grand Unified Theories, which attempt to describe the unification of the known
75 forces, predict rates for proton decay that cover a range directly accessible with the next
76 generation of large underground detectors such as the ELBNF detector. The experi-
77 ment's sensitivity to key proton decay channels will offer unique opportunities for the
78 ground-breaking discovery of this phenomenon.

79 Neutrinos emitted in the first few seconds of a core-collapse supernova carry with
80 them the potential for great insight into the evolution of the Universe. ELBNF's capa-
81 bility to collect and analyze this high-statistics neutrino signal from a supernova within
82 our galaxy would provide a rare opportunity to peer inside a newly-formed neutron star
83 and potentially witness the birth of a black hole.

84 To achieve its goals, ELBNF is centered around three central components: (1) a
85 new, high-intensity neutrino source generated from a megawatt-class proton accelerator
86 at Fermi National Accelerator Laboratory (Fermilab), (2) a fine-grained near neutrino
87 detector installed just downstream of the source, and (3) a massive liquid argon (LAr)
88 time-projection chamber (TPC) deployed as a far detector deep underground at the
89 Sanford Underground Research Facility (SURF). This facility, located at the site of the
90 former Homestake Mine in Lead, South Dakota, is \sim 1,300 km from the neutrino source
91 at Fermilab - a distance (baseline) that delivers optimal sensitivity to neutrino charge-
92 parity symmetry violation and mass ordering effects. This ambitious yet cost-effective
93 design incorporates scalability and flexibility and can accommodate a variety of upgrades
94 and contributions.

95 ELBNF plans to place modular LAr TPCs with a combined total fiducial mass of at
96 least 40 kton in the underground facility at Homestake and into the neutrino beam. The
97 first 10 kton LAr TPC module is planned to be constructed underground on the time
98 scale of 2021.

99 With its exceptional combination of experimental configuration, technical capabili-

ties, and potential for transformative discoveries, ELBNF promises to be a vital facility for the field of particle physics worldwide, providing physicists from institutions around the globe with opportunities to collaborate in a twenty to thirty year program of exciting science.

1.1 Key physics goals of ELBNF

The primary goal of ELBNF is to measure the appearance of electron neutrinos in a beam of muon neutrinos and the appearance of electron anti-neutrinos in a beam of muon anti-neutrinos, each over the 1300 km baseline of the experiment. Precise measurement of this phenomenon would allow for determination of the relative masses and mass ordering of the three known neutrinos. Measurement of these neutrino oscillation channels also allow to constrain or measure the CP violation phase, δ_{CP} in the neutrino sector, which is possibly connected to the dominance of matter over antimatter in the universe.

For a baseline of 1300 km the first maximum of the oscillation probability occurs in the 2 - 3 GeV energy range with additional oscillation maxima at lower energies. Hence the high intensity neutrino flux must be peaked in this energy range. Coverage of the sub GeV energy range is desirable to potentially map out the second maximum in the oscillation probability. It is this key physics which dictates the neutrino energy range and thereby the energy range of charged particles which result from neutrino interactions in the ELBNF detectors.

1.2 Single-phase LAr detector

The basic components of the liquid argon detector include a cryostat and associated cryogenic system. A time projection chamber (TPC) and readout electronics are housed in the cryostat.

The cryostat contains the liquid argon target material and the cryogenic system keeps the liquid argon at a cryogenic temperature of 89K, and maintains the required purity through pump and filter system. A uniform electric field is created within the TPC volume between cathode planes and anode wire planes. Charged particles passing through the TPC release ionization electrons that drift to the anode wires. The bias voltage is set on the anode plane wires so that ionization electrons drift between the first several (induction) planes and is collected on the last (collection) plane. Readout electronics amplify and continuously digitize the induced waveforms on the sensing wires at several MHz, and transmit these data to the DAQ system for analysis. The wire planes are oriented at different angles allowing a 3D reconstruction of the particle trajectories. In addition to these basic components, a photon detection system is also included in the design to enable the study of proton decay and be sensitive to galactic supernova neutrinos.

The LAr detector design is characterized by a modular approach in which the LAr volume in the cryostat is instrumented with a number of identical anode wire plane assemblies (APA) and associated cathode plane assemblies (CPA). To a large extent, scaling from detector volumes containing from a few to several hundred of such modules should be straightforward with small and predictable risk.

141 1.3 Goals for the prototype detector and beam test

142 The physics sensitivity of ELBNF has been estimated based on detector performance
143 characteristics published in the literature, simulation based estimates as well as a vari-
144 ety of assumptions about the anticipated performance of the future detector and event
145 reconstruction and particle identification algorithms. The proposed single phase LAr
146 prototype detector and CERN beam test aim to replace these assumptions with mea-
147 surements for the full scale ELBNF detector components and the presently available
148 algorithms. Thereby the measurements will allow to enhance the accuracy and reliabil-
149 ity of the ELBNF physics sensitivity projections. The beam measurements will serve
150 as a calibration data set to tune the Monte Carlo simulations and serve as a reference
151 data set for measurements of the future ELBNF detector. In addition, the measurement
152 program aims to evaluate and benchmark the performance of the detector and its indi-
153 vidual components. This will allow to identify potentially problematic components and
154 lead to future improvements and optimizations of the detector design.

155 In order to make such precise measurements, the detector will need to accurately
156 identify and measure the energy of the particles produced in the neutrino interaction
157 with Argon which will range from hundreds of MeV to several GeV. To mitigate the
158 risks associated with extrapolating small scale versions of the single-phase LAr TPC
159 technology to a full-scale detector element, it is essential to benchmark the operation of
160 a full-scale detector elements in a well characterized charged particle beam.

161 More specifically, the goals of the prototype detector and beam test measurements
162 include the the use of a charged particle beam to:

- 163 1. measure the detector calorimetric response for
 - 164 (a) hadronic showers
 - 165 (b) electromagnetic showers
- 166 2. study e/ γ -separation capabilities
- 167 3. measure event reconstruction efficiencies as function of energy and particle type
168 based on experimental data
- 169 4. measure performance of particle identification algorithms as function of energy and
170 for realistic detector conditions
- 171 5. assess single particle track calibration and reconstruction
- 172 6. validate accuracy of Monte Carlo simulations for relevant energy ranges as well as
173 directions
- 174 7. study other topics with the collected data sets
 - 175 (a) pion interaction kinematics and cross sections
 - 176 (b) kaon interaction cross section to characterize proton decay backgrounds ...
 - 177 (c) muon capture for charge identification

178 For the detector performance characterization a well defined charged particle test
179 beam will enable the following detector performance measurements:

- 180 1. characterize performance of full scale TPC module
- 181 2. verify functionality of cold TPC electronics under LAr cryogenic conditions
- 182 3. perform full-scale structural test under LAr cryogenic conditions
- 183 4. study performance of the photon detection system
- 184 5. verify argon contamination levels and associated mitigation procedures
- 185 6. develop and test installation procedures for full-scale detector components
- 186 7. test and evaluate the performance of detector calibration tools

187 The CERN charged particle beam lines provide an opportunity to perform this crucial
188 test of the proposed single-phase LAr TPC and thereby inform the decision regarding
189 the far detector design and layout for ELBNF. In order to be of greatest value to this
190 decision making process results should be available as soon as possible.

191 This technical document describes the motivation and technical details for an initial
192 measurement program that we propose to be executed by mid 2018, that is *before* the
193 anticipated LHC long shutdown. The estimated required beam time amounts to \sim XX
194 weeks of data collection. Additional follow-up measurements with potentially modified
195 detector components form a potential extension to the proposed program.

196 2 CERN prototype detector and charged particle 197 beam test [\sim 10 pages; **Donna/Jarek**]

198 TODO list

199 **Sensitivity plots.** Create plots for the CPV and HM sensitivities for 40kton detector
200 and 1.2 MW beam. Plots should include various combinations of the assumed
201 uncertainties: with current best measurements, with best guesses about uncer-
202 tainties we can archive and with uncertainties which will be obtain using beam
203 test experiment at CERN.

204 **E-m shower calibration energy scale.** Estimate statistics of particles to optimise
205 the measurement of EM showers. Provide the necessary statistics as a function of
206 energy. Optimise the energy bins widths, where we expect coarser bins for higher
207 energies than for lower energies.

208 **Hadronic shower calibration** Estimate statistics of particles to optimise the mea-
209 surement of hadronic showers. Provide the necessary statistics as a function of
210 energy. Optimise the energy bins widths, were we expect coarser bins for higher
211 energies than for lower energies.

212 Estimate pi0 production from the proton scattering in the TPC.

- 213 **Reconstruction issues.** Obtain values for the uncertainties due to finding vertex po-
 214 sition of neutrino interactions.
 215 Estimate statistics necessary to improve low energy electrons acceptance due to
 216 reconstruction algorithms limitations.
- 217 **e/gamma separation** Estimate statistics necessary for improvement of the e/gamma
 218 separation. Assume three values for wire pitch: 3mm, 4mm and 5mm.
- 219 **Pion cross sections: absorption, charge exchange in Ar** Get statistics for pions
 220 to measure their cross sections. Estimate energy bin widths.
- 221 **Kaon cross section in Ar** Get statistics for kaons to measure their cross sections.
 222 Estimate energy bin widths.
- 223 **Muon capture** Estimate statistics for antimuons for capture on argon to be used for
 224 the statistical determination of the wrong sign neutrino contribution on the beam.

225 2.1 Requirements for the detector, beam and commissioning

226 The Single-Phase Cern Prototype detector is intended to provide necessary information
 227 to reduce systematic uncertainties for the oscillation measurements in the US-based
 228 long base-line neutrino experiment. The LAr TPC technology is not new but wasn't
 229 extensively used in the 1-10 GeV neutrino energy range. The main source of uncertainties
 230 due to detector with the current values are shown in table 1

Table 1: Current known sources of detector uncertainties for liquid argon or TPC.

| source of uncertainty | value | reference |
|---|-------|-----------|
| e/ γ separation | | |
| e-m shower calibration | | |
| hadronic shower calibration | | |
| low energy acceptance electron identification | | |
| | | |

Table 2: Current known sources of uncertainties due to interaction of charged particle with argon.

| source of uncertainty | value | reference |
|--|-----------------------|-----------|
| pion(Kaon) absorbtion | | |
| pion(Kaon) charge exchange | | |
| pion (Kaon) production in secondary interactions | | |
| muon capture | Phys. Rev. C 35, 2212 | |
| energy scale | | |
| Michel electron tagging | | |
| | | |

231 With current detector uncertainties from table 1 the sensitivities for the CP violation
232 phase measurement is shown in Fig. 2.1 **Task: make this plot**. The proposed test
233 beam detector will reduce uncertainties to XX% and improve our sensitivity to δ_{CP} as
234 shown in Fig. 2.1 **Task: make this plot**.

Figure 1: Sensitivities for the δ_{CP} measurement for using current knowledge of the single-phase LAr-TPC detector technology and for reduced detector uncertainties from SPCP beamtest data. The plots prepared for 40 kton fiducial mass and $xx \times 10^{21}$ POT.

235 **2.1.1 Particles energy and direction**

236 Plans for running beam for the the ELBNF include both neutrino and anti-neutrino
237 configurations. These beams will be composed mainly of muon neutrinos (anti-neutrinos)
238 as well as electron neutrinos (anti-neutrinos). In figures 2.1.1 and 2.1.1 the distributions
239 on momenta and angles of particles created in neutrino interaction are shown.

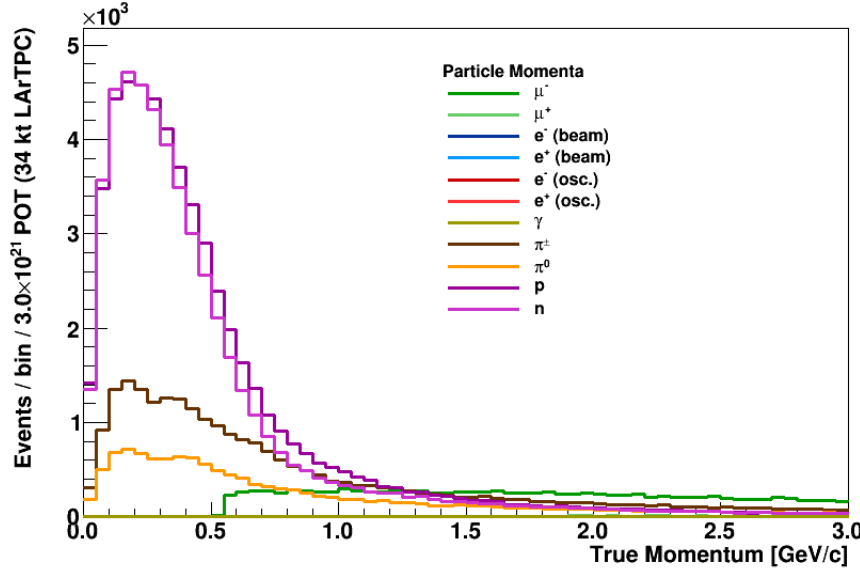


Figure 2: Particle momenta distributions for particles coming from all fluxes (ν_e , ν_μ , $\bar{\nu}_e$ and $\bar{\nu}_\mu$) at both near and far detector locations.

Figure 3: Particle angle wrt to the beam axis distributions for particles coming from all fluxes (ν_e , ν_μ , $\bar{\nu}_e$ and $\bar{\nu}_\mu$) at both near and far detector locations.

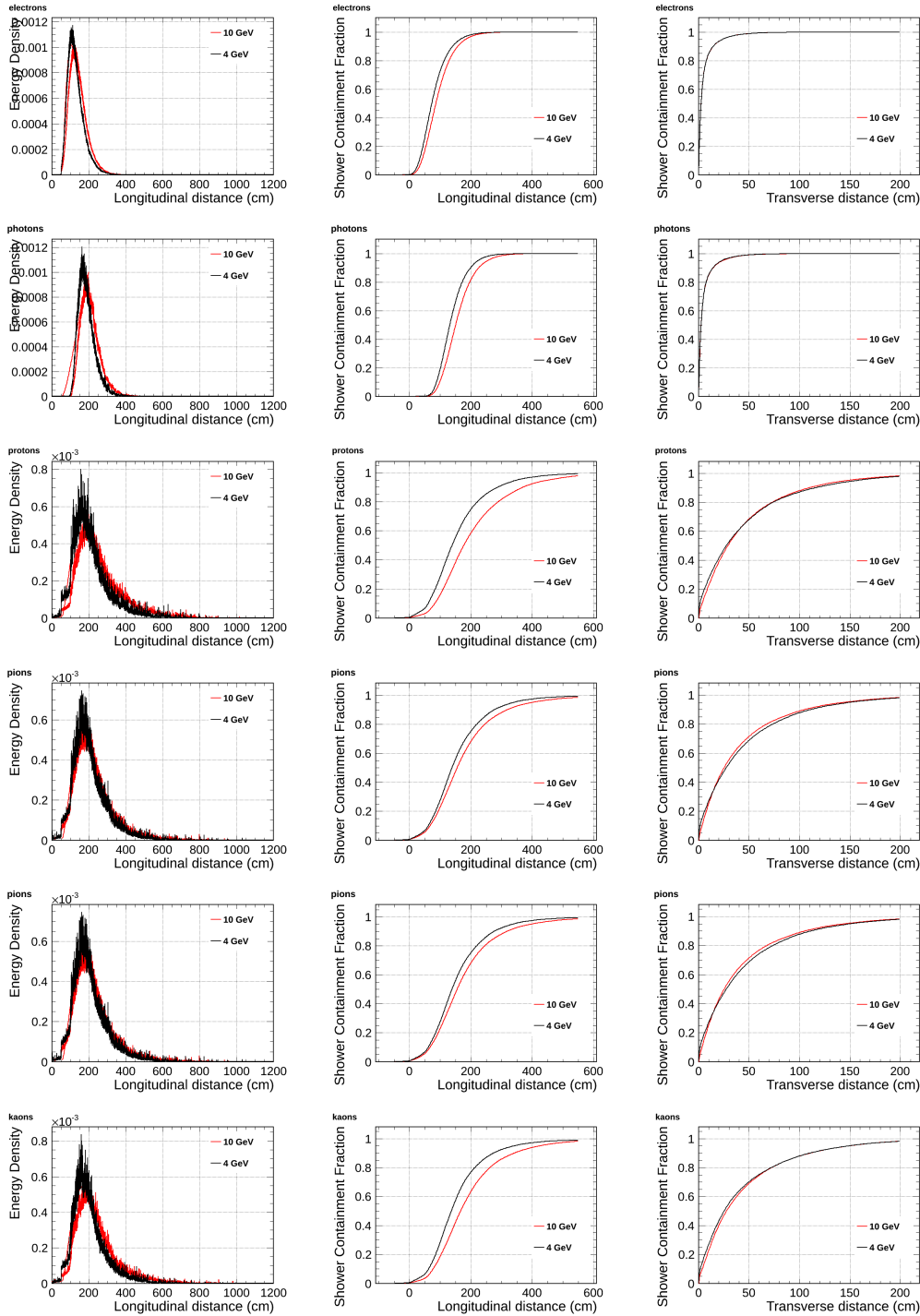


Figure 4: Particle containment plots.

240 **2.1.2 Run plan**

Table 3 summarizes the required exposures to beam particles.

| Particle | Momenta (GeV) | Exposure | Purpose |
|---------------|---|----------|----------------------------|
| charged π | 0.1, 0.2, 0.3, 0.4, 0.5, 1, 2, 3, 5, 10 | 10K | hadronic shower |
| charged π | 1 | 10K | vary angle, reconstruction |
| electron | 0.1, 0.2, 0.3, 0.4, 0.5, 1, 2, 3, 5, 10 | 10K | EM shower/e- γ PID |
| electron | 1 | 10K | vary angle, reconstruction |
| muon | 0.1, 0.3, 0.5, 1, 2, 5, 10 | 10K | E_μ calibration, MCS |
| muon | 1 | 10K | vary angle, reconstruction |
| proton | 0.1, 0.2, 0.3, 0.5, 1, 2 | 10K | response, PID |
| proton | 1 | 10K | vary angle, reconstruction |
| kaon | 0.1, 0.2, 0.3, 0.5, 1 | ? | response, PID |

Table 3: Run plan requirements.

241
242 NUMBERS ARE UPDATED GUESSES - STUDIES NEEDED HERE

243 Charged pion samples will be used to characterize hadronic shower response and to
244 measure absorption cross section parameters on argon. Muon samples will be used for
245 calibration and reconstruction tests. Electron samples will be used to measure EM
246 shower response and to tune PID algorithms. Proton response will be studied for
247 reconstruction and to tune PID algorithms. Kaon data will be needed to tune proton
248 decay backgrounds . Special runs at various angles with π , μ , p and electrons will be
249 performed to study reconstruction and tune PID algorithms.

250 **2.2 Detector performance tests**

251 **2.2.1 Bethe-Bloch parametrisation of charged particles**

252 The SPCP will allow to study the detector response to charge particles from the test
253 beam and will serve as a calibration detector. The measured energy deposition for
254 various particles and its dependence on the direction of the particle will feed into our
255 Monte Carlo generator and allow more precise reconstruction of neutrino energy and
256 interactions topologies with good particle identifications.

257 **How we compare with Lariat? Multiple scattering**

258 The set of single-phase prototype detector helped to understand the detector response
259 to cosmic muons. But there is still lots to learn with additional studies. The charge
260 particle identification efficiencies has been mapped for only limited range of the particle
261 energies.

262 **2.2.2 e/ γ separation**

263 The separation of the electrons from photons is the most important feature of the LAr
264 TPC detectors for the search of the CP violation phase where we look for appearance
265 of the ν_e in the ν_μ beam. Showers from electrons are part of the signal whilst the single
266 photons might contribute to the background sample. The photons can undergo two
267 process: pair production and Compton scattering. The dominant process for photons

268 with energies of several hundreds MeV is the $e^+ e^-$ pair production, but Compton scat-
269 tering also occur at this energies. For pair production the e/γ separation is achieved by
270 looking at the beginning of the electromagnetic shower, where for election we see energy
271 deposition typical for single MIP and for photon we see energy deposition consisted with
272 two MIP. The separation of e/γ has been measured in the ArgoNEUT experiment using
273 neutrino scattering data with low statistics. Currently the separation efficiency is esti-
274 mated to be at the level of of 94 % (? cite and check the number). In case of Compton
275 scattering off of atomic electrons the signal is much more difficult to distinguish from
276 the CC ν_e scattering signal.

277 The separation of the e/γ measured by ArgoNEUT is not sufficient for the ELBNF
278 experiment. Here we propose a measurement of the separation efficiency as the function
279 of energy and angle. **we need someone to look into this**

280 2.2.3 Reconstruction efficiencies and particle identification

281 The reconstruction of events in the LAr TPC is still a challenge but rapid progress has
282 been achieved in recent years (cite pandora and other reconstruction algorithms). De-
283 spite the progress reconstruction algorithms have to rely Monte Carlo predictions which
284 don't simulate liquid argon detectors responses correctly. Reconstruction algorithms
285 will benefit greatly from test beam data particularly from the full scale prototype. The
286 reconstruction algorithms will be trained to correctly reconstruct track, electromagnetic
287 and hadronic showers. The data of tracks and showers can be used to create a library
288 of reference events with which to tune algorithms.

289 Main issues for the reconstruction algorithms:

- 290 • The reconstruction algorithms try to use all three planes on the signal readout. if
291 the orientation of the track/shower is such that it is aligned with wires on one of
292 the plans it significantly reduces quality of reconstructed objects.
- 293 • Calorimetry with collection and induction planes. In the ICARUS experiment the
294 deposited energy was reconstructed from the signal on the collection plane. The
295 induction planes bipolar signal wasn't "stable" enough to use it for calorimetric
296 measurement. In the ELBNF design there is additional shielding wire plane which
297 will improve the quality of the bipolar signal and the test beam experiment will
298 help with its calibration.
- 299 • Vertexing.
- 300 • Reconstruction efficiency for low energy particles. The reconstruction algorithm
301 suffer from the lose of fefficiency for low energy particle or particles which leave
302 less than 200-300 hits. Training the algorithms on a low energy particles from the
303 test beam will improve the quality and efficiency of the reconstructed objects.

304 2.2.4 Cross section measurements

305 Precise measurement of the absorption and charge exchange of pions and kaons. Pion
306 absorption is a large part of the pion nucleon cross section from 50 MeV to 500MeV with

307 no data above about 1GeV pion kinetic energy. **Add plots and values for known**
308 **cross sections wit errors**

- 309 • pion absorption on argon - Kotlinski, EPJ 9, 537 (2000)
310 • pion cross section as a function of A - Gianelli PRC 61, 054615 (2000)

311 There is not currently a satisfactory theory describing absorption. The Valencia group
312 (Vicente-Vacus NPA 568, 855 (1994)) developed model of the pion-nucleus reaction with
313 fairly good agreement, although not in detail. The actual mechanism of multi-nucleon
314 absorption is not well understood.

315 **2.2.5 Charge sign determination**

316 It is not possible to determine charge of the particle on the event by event basis with
317 non-magnetised LAr TPC detectors. A statistical separation will be studied which will
318 make use of differences in muon versus antimuon capture cross sections and lifetime. For
319 the μ^+ for argon we expect about xx% to be captured and for μ^- about yy%.

320 **2.2.6 Single track calibration**

321 **2.2.7 Shower calibration**

322 Reconstruction of neutrino energy depends of a quality of reconstruction of both elec-
323 tromagnetic and hadronic showers.

324 - **features of Hadronic shower in LAr TPC** - **features of electromagnetic**
325 **shower in LAr TPC** - Missing energy from neutral (Neutrons scattering)

326 **2.3 Other measurements**

327 **2.3.1 Anti-proton annihilation**

328 **2.3.2 Proton decay background (cosmogenic $K^0 \rightarrow K^+$)**

329 **3 Single Phase LAr Detector [\sim 10 pages; J. Stewart
330 et al.]**

331 **3.1 ELBNF detector**

332 The far detector for the ELBNF collaboration will be a series of four liquid argon time
333 projection chambers (TPC), each in a cryostat that holds a fiducial/active/total LAr
334 mass of 10.0/13.3/16.9 kt. The TPCs will be instrumented with photon detection. It is
335 planned that the first 10 kt detector will be ready for installation in the 2021 timeframe.
336 One option for the TPC design is a wire plane based TPC with cold electronics readout.
337 Designs of this style are referred to as single-phase detectors as the charge genera-
338 tion, drift, and detection all occurs in the argon liquid phase. This style TPC has the
339 advantage that there is no charge amplification before collection making a very precise
340 charge measurement possible. To achieve ELBNF's goals, a detector much larger than

341 ICARUS, the largest LAr TPC detector built to date, is needed. The LBNE experiment
 342 was developing a scalable far detector design shown in Figure 5 that would scale-up LAr
 343 TPC technology by roughly a factor of 40 compared to the ICARUS T600 detector.
 344 To achieve this scale-up, a number of novel design elements need to be employed. A
 345 membrane cryostat typical for the liquefied natural gas industry will be used instead of
 346 a conventional evacuated cryostat. The wire planes or anode plane assemblies (APAs)
 347 will be factory-built as planar modules that are then installed into the cryostat. The
 348 modular nature of the APAs allow the size of the detector to be scaled up to at least
 349 40 kt fiducial mass. Both the analog and digital electronics will be mounted on the wire
 350 planes inside the cryostat in order to reduce the electronic noise, to avoid transporting
 351 analog signals large distances, and to reduce the number of cables that penetrate the
 352 cryostat. The scintillation photon detectors will employ light collection paddles to re-
 353 duce the required photo-cathode area. Many of the aspects of the design will be tested
 354 in a small scale prototype at Fermilab but given the very large scale of the detector el-
 355 ements a full-scale test is highly desirable. As the new ELBNF collaboration forms and
 356 organized a combined detector design team will emerge. Ideas from this new collabora-
 357 tion will modify the design presented here but this design provides a concrete example
 358 of a possible future detector.

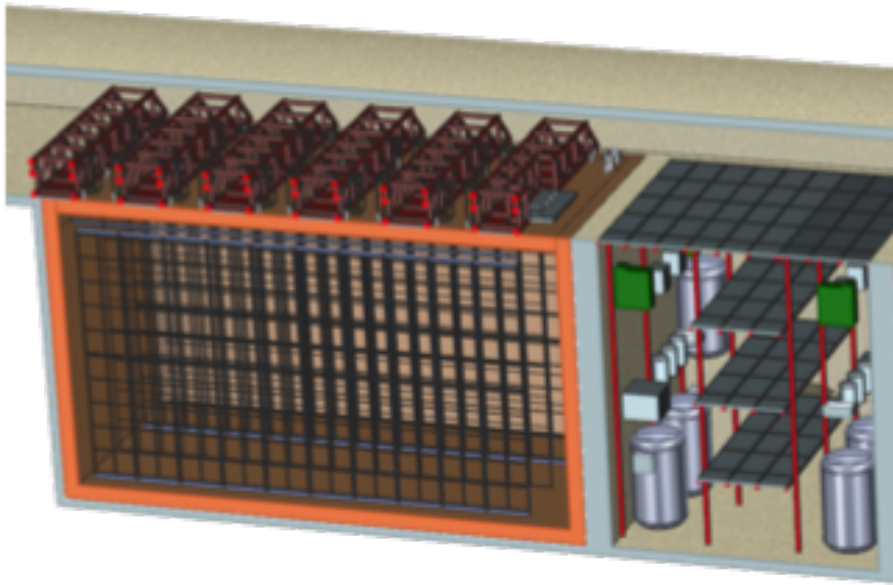


Figure 5: 3D model of one design of the ELBNF single-phase detector. Shown is 5kt fiducial volume detector which would need to be lengthened for the 10 kt design. The present ELBNF plan calls for the construction of 4 10 kt detectors of similar design.

359 The goals of the ELBNE detector test can be broken into four categories: argon
 360 contamination mitigation verification, TPC mechanical verification, TPC electrical veri-
 361 fication, and photon detection light yield verification. Research at Fermilab utilizing the
 362 Materials Test Stand has shown that electronegative contamination to the ultra-pure
 363 argon from all materials tested is negligible if the material is under the liquid argon.
 364 This implies that the dominant source of contamination originates from the gas ullage
 365 region and in the room temperature connections to the detector. Careful design of the

ullage region to insure that all surfaces and feedthroughs are cold is expected to greatly
 reduce the sources of contamination over what exists in present detectors. Other con-
 cepts attempt to eliminate the gas ullage completely. The goals related to mechanical
 testing are to test the integrity of the detector. In the current design, each APA mea-
 sures 2.3 m by 6.0 m and includes 2560 wires and associated readout channels. Given
 the complexity of these assemblies, a test where the detector can be thermally cycled
 and tested under operating conditions is highly advised prior to mass production. The
 mechanical support of the APAs can be tested to verify that the mechanical design is
 reliable and will accommodate any necessary motion between the large wire planes. The
 impact of vibration isolation between the cryostat roof and the detector can also be
 tested. Finally a potential improvement in the cryostat design is the possibility to move
 the pumps external to the main cryostat. This will reduce any mechanical coupling to
 the detector and also greatly improve both reliability and ease of repair. The electrical
 testing goals are to insure that the high voltage design is robust and that the required
 low electronic noise level can be achieved. As the detector scale increases so does the
 capacitance and the stored energy in the device. The design of the field cage and high
 voltage cathode planes needs to be such that HV discharge is unlikely and that if the
 event occurs no damage to the detector or cryostat results. The grounding and shielding
 of large detectors is also critical for low noise operation. By testing the full scale ele-
 ments one insures that the grounding plan is fully developed and effective. Large scale
 tests of the resulting design will verify the electrical model of the detector.

3.2 CERN prototype detector

3.2.1 Overview of the CERN Single-Phase test Detector

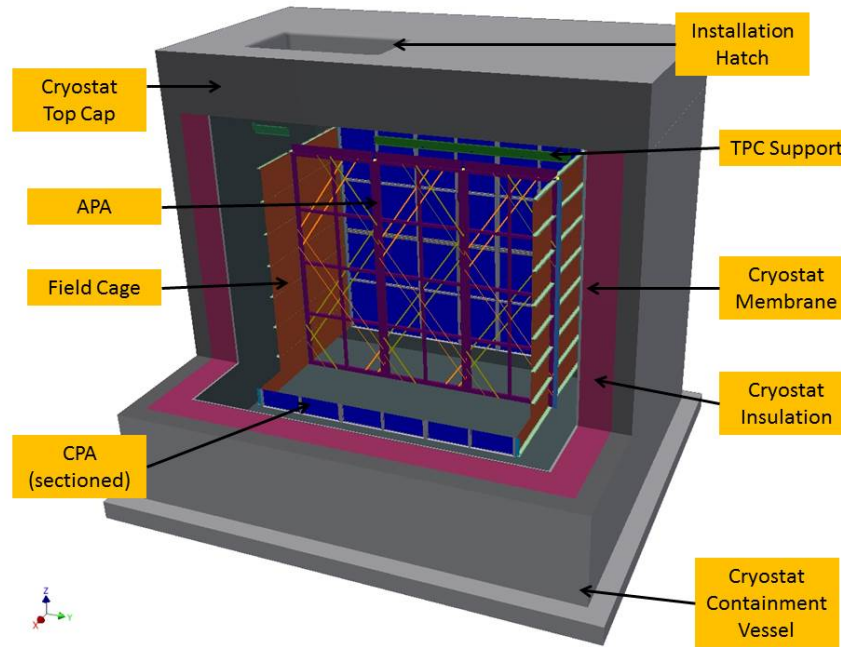


Figure 6: 3D model of the single-phase detector prototype is shown inside the test cryostat.

389 This sections presents the design details of a single-phase detector based on the
390 development of the LBNE collaboration. As ELBNF moves forward the TPC working
391 group will evaluate this and any modifications or alternate proposals. For the purpose
392 of this proposal this represents one alternate, and it is expected to evolve as the new
393 collaboration organized and more work is done.

394 This TPC consists of alternating anode plane assemblies (APAs) and cathode plane
395 assemblies (CPAs), with field-cage panels enclosing the four open sides between the
396 anode and cathode planes. Figure 6 shows a sectioned view for the planned TPC inside
397 the cryostat at CERN. A uniform electric field is created in the volume between the anode
398 and cathode planes. A charged particle traversing this volume leaves a trail of ionization.
399 The electrons drift toward the anode plane, which is constructed from multiple layers of
400 sense wires, inducing electric current signals in the front-end electronic circuits connected
401 to the wires.

402 To the extent possible the TPC will be assembled from elements that are of the
403 same size as those planned for the single phase far detector. The primary exception to
404 this is the length of the field cage panels which are 2.5m in this design, compared to
405 3.4m in the far detector. This is because the drift distance between the APA and CPA is
406 reduced to lessen the impact of space charge on the prototype necessitated by the surface
407 operation. The overall size of the TPC will be derived by the size and number of anode
408 planes (APA). It has been determined in order to perform the required physics, the TPC
409 will have a 3-APA wide active volume. The APAs will have an active (total) area 2.29 m
410 (2.32 m) wide and 6.0 m (6.2 m) high. The combination of the three APAs determines
411 the overall TPC length to be 7.2 m. There will be a cathode plane (CPA) on either side
412 of the APAs. The overall width of the TPC will be determined by a combination of the
413 drift distances along with the thickness of the APA, which is constructed of 76.2 x 101.6
414 mm stainless steel (SS) structural tubing. The overall width of the TPC is 5.2 m. Like
415 the length of the TPC, the overall height will be determined by the height of the APA
416 which is 6.3 m. In summary the external TPC dimensions will be 7.2 m long x 5.2 m
417 wide x 6.3 m high. Along with the APAs and CPAs, the TPC will include a field cage
418 that surrounds the entire assembly. This is a series of pultruded fiberglass I beams for
419 the structural elements. These I-beams will be tiled with large copper sided FR4 panels
420 to create the field cage. Each panel will be connected with a series of resistors. The field
421 cage will be connected to the CPAs through a capacitor assembly.

422 All of this will be supported by rows of I-beams supported from a mechanical struc-
423 ture above the cryostat. The hangers for these I-beams will pass through the insulated
424 top cap. There will be a series of feed thru flanges in the top cap of the cryostat to bring
425 in and take out services for the TPC. There will be a HV feed thru for each of the CPA
426 rows and one signal feed thru for each of the APAs.

427 The minimum internal size of the cryostat is 9.5 m long, 7.3 m wide and 8.4 m high.
428 This is determined from size of the TPC. These dimensions also preserve the ability to
429 reverse the order of the APAs and CPAs inside the TPC. The current plan is to have
430 the APAs located in the center of the cryostat with a CPA on each side. Reversing this
431 to have the CPA in the center and APAs on each side may be required to minimize the
432 dead space between the two drift volumes.

⁴³³ **3.2.2 Anode Plane Assemblies (APAs)**

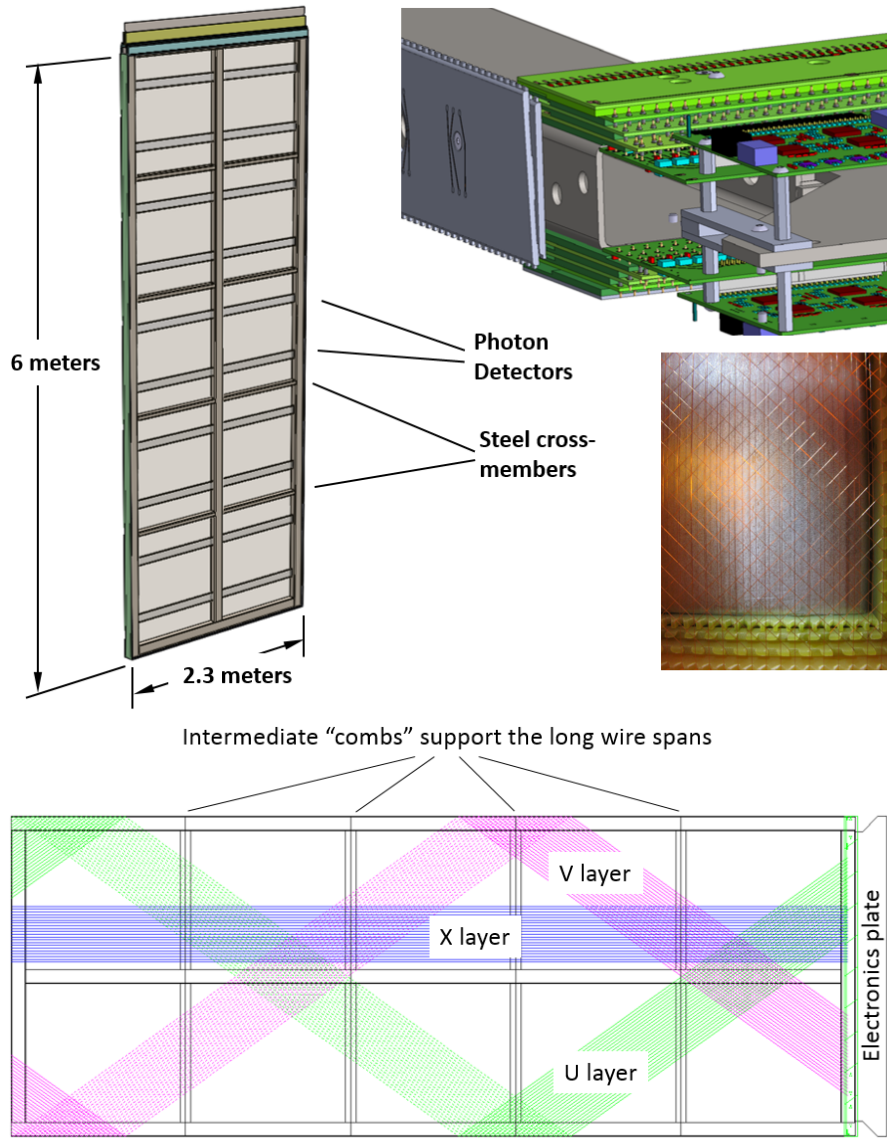


Figure 7: Clockwise from left: A full size APA, an APA corner showing the electronics boards, an APA lower corner photo showing wires and edge boards, and a figure showing the wire orientations and the placement of wire aligning combs.

⁴³⁴ Each APA (Figure 7) is instrumented with 3 layers of signal wires, one longitudinal
⁴³⁵ collection plane and two 35.7° angled induction planes with an additional outer grid plane
⁴³⁶ that helps maintain the field. The overall dimensions of the active area as mentioned
⁴³⁷ are 2.3 m wide, 6 m long. The dimension of the wire planes were selected to fit down
⁴³⁸ the Ross shaft at SURF, be compatible with a standard HiCube transport container,
⁴³⁹ and allow construction from readily available materials. The angled layers start at the
⁴⁴⁰ electronics end and wind around to the other side on their way to the bottom. The wire
⁴⁴¹ angle was selected so that a given angled induction wire will not overlay any longitudinal
⁴⁴² collection wire more than once in order to reduce ambiguities caused by the wrapped

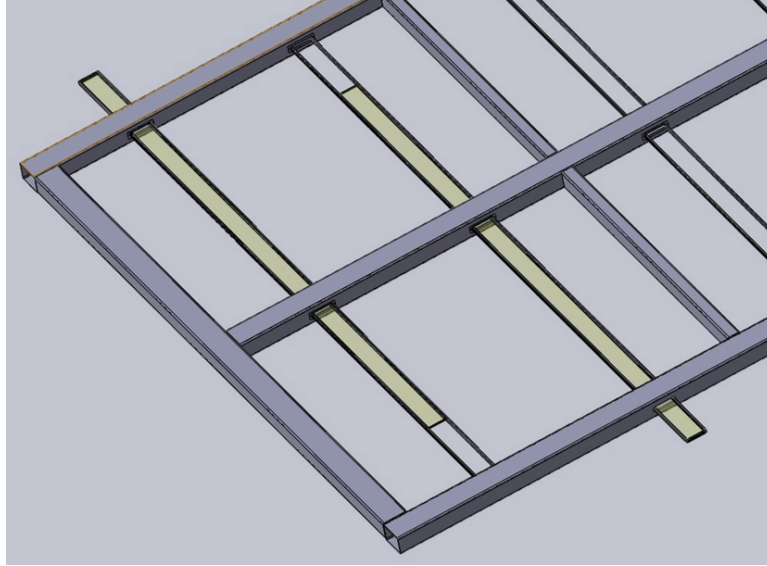


Figure 8: Photon detectors are mounted within the frame, between the wires on the two sets of four wire layers. The APA is built so that the photon detectors can be installed through slots in the side of the APA after the APA wires are installed. The wires that would cross these slots are routed around using copper traces on the edge boards.

wire construction. Partial wire layers are shown here in Figure 7 at the bottom. With
 443 a wire pitches of 4.67 mm (diagonal layers) and 4.79 (straight layers), the total number
 444 of readout channels in an APA is 2560. The grid layer is not depicted in Figure 7 for
 445 clarity. The underlying structure of each APA is a framework of rectangular, stainless
 446 steel tubing. The side and bottom edges of the frame are lined with multiple layers of
 447 fiberglass circuit boards, notched along the edges to support and locate the wires that
 448 cross the APA face. A set of FR4 combs are glued to the APA frame to capture the
 449 wires at regular intervals. The front-end electronics boards are mounted at the top end
 450 of the frame and protected by a metal enclosure.
 451

The distance between wire planes is 4.8 mm (3/16 in) corresponding with standard
 452 printed circuit board thickness, and while maintaining optimal signal formation. The
 453 four wire planes will be electrically biased so that electrons from an ionizing-particle
 454 track completely drift past the first three planes and are collected by the fourth plane.
 455 Calculations show that the minimum bias voltages needed to achieve this goal are V_G
 456 = -665V, V_U = -370V, V_V = 0V and V_X = 820V respectively (where G, U, V, and X
 457 are the wire-layer labels from outside in, towards the frame). It is convenient to set
 458 one of the wire planes to ground so that the wires can be DC coupled to the front-end
 459 readout electronics. In this instance, the V wire plane is set to ground potential to
 460 reduce the maximum bias voltages on the other wire planes, and enable the use of lower
 461 voltage rated AC coupling capacitors. A grounded mesh plane, located 4.8 mm behind
 462 the collection (X) plane, prevents the electric field around this set of wires from being
 463 distorted by the metal frame structure and the wires on the opposite side of the frame. It
 464 also shields the sensing wires from potential EM interferences from the photon detectors
 465 (Fig. 3.2.2) mounted within the frame. The mesh should have a wire pitch less than 2
 466 mm to ensure a uniform electric field while maintaining a high optical transparency.
 467

468 **3.2.3 CPA and Field Cage**

469 Each cathode plane (Fig. 9) is constructed from 6 identical CPA (cathode plane assem-
470 bly) modules and two sets of end pieces. Each CPA is about half the size of an APA
471 (2.3m × 3.1m) for ease of assembly and transport. The CPA is made of a stainless-steel
472 framework, with 4 pieces of thin FR4 sheets mounted in the openings. A receptacle for
473 the HV feedthrough is attached to the upper corner of a cathode plane toward the roof
474 entrance side to mate with the HV feedthrough in the cryostat ceiling.

475 The FR4 sheets on the CPAs are treated with layers of high resistive coating on both
476 sides. The resistivity of the coating will be chosen such that the surface potential does
477 not deviate significantly with the ionization current from the cosmic rays, and forms a
478 relatively long time constant to dissipate the stored energy on each sheet in case of a
479 high voltage discharge. This long RC time constant will also reduce the peak current
480 injected into the front-end electronics in a HV discharge.

481 Due to the relatively high cosmic ray flux in this surface detector, it is preferable to
482 prevent the scintillation light emitted by a cosmic ray between the cathode and cryostat
483 wall from entering the TPC to reduce false trigger. The opaque cathode surface will
484 service this purpose. The high flux of cosmic rays combined with very low drift velocity
485 of positive ions in the liquid argon will result in sizable space charge distortions in
486 the TPC (docdb #6471). In addition, the positive ions could build up further if the
487 ion motion is slowed or stalled by counter flow in the LAr. Preliminary CFD analysis
488 (docdb #6140) have shown that solid cathodes in the cryostat result in LAr flow pattern
489 that neither causes excess positive ion buildup, nor degrades the LAr purity.

490 To achieve a 500 V/cm drift field over a 2.5 m distance, the bias voltage on the
491 cathode plane must reach −125 kV. Two high voltage power supplies (150 – 200 kV) and
492 two HV feedthroughs will be needed for the two cathode planes. The HV feedthroughs
493 are based on the Icarus design, but modified to further improve the stability at higher
494 voltages.

495 Each pair of facing cathode and anode rows forms an electron-drift region. A field
496 cage completely surrounds the four open sides of this region to provide the necessary
497 boundary conditions to ensure a uniform electric field within, unaffected by the presence
498 of the cryostat walls.

499 The field cages are constructed using copper-clad FR4 sheets reinforced with fiber
500 glass I-beams to form panels of 2.5 m × 2.3 m in size for the top and bottom modules,
501 and 2.5 m × 2 m modules for the sides. Parallel copper strips are etched or machined
502 on the FR4 sheets. Strips are biased at appropriate voltages through a resistive divider
503 network. These strips will create a linear electric-potential gradient in the LAr, ensuring
504 a uniform drift field in the TPC’s active volume.

505 Since the field cage completely encloses the TPC drift region on four (of six) sides,
506 with the remaining two sides blocked by the solid cathodes, the FR4 sheets must be fre-
507 quently perforated to allow natural convection of the liquid argon. The “transparency”
508 of the perforation will be determined by a detailed LAr computerized fluid dynamic
509 (CFD) study.

510 The left of Figure 10 shows a section of the field cage in the 35ton TPC as it was
511 being assembled. The 35ton TPC test results will inform us whether we should improve
512 upon the current design, or change the design concept all together for this and future

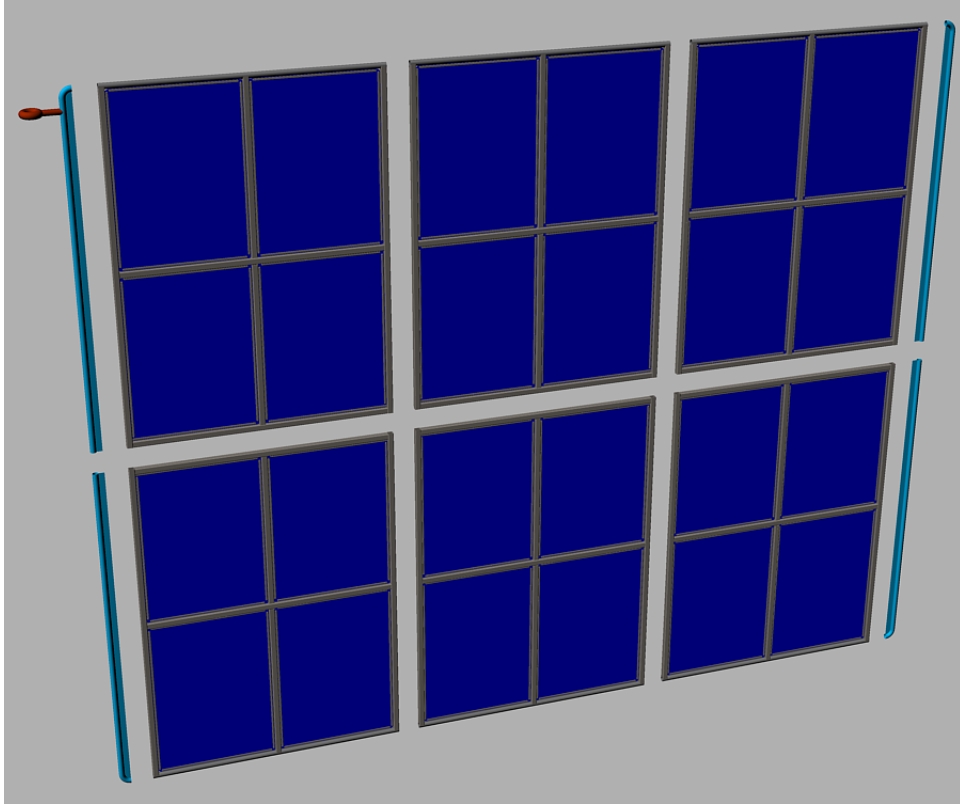


Figure 9: Exploded view of a cathode plane constructed from 6 CPA modules and 4 end pieces. The facing material on the CPA is highly resistive to minimize the peak energy transfer in case of a HV breakdown.

513 detectors. The main concern with the current field cage design is that the electric field
 514 at the edges of the copper strips is still quite high due to the thinness of the copper.
 515 One possible remedy is to cover the entire surface of the field cage with a high resistive
 516 coating. The resistivity between strips due to this coating must be kept many orders
 517 of magnitudes higher than the divider resistance to avoid distortion to the drift field.
 518 Figure 10 (Right-Panel) shows an FEA simulation of such a configuration.

519 In the event of HV discharge on the cathode or the field cage, the voltage differential
 520 between neighboring field cage strips near the discharge electrode will be very high
 521 for a brief moment. This over voltage condition could cause damage to the field cage
 522 electrode and the resistors installed between strips. To minimize such risk, varistors or
 523 gas discharge tubes (GDT) will be installed between the field cage strips in parallel with
 524 the resistors to prevent excess voltage transient between the electrodes.

525 In order to test the installation concept of the far detector, the top and bottom field
 526 cage modules will be attached to the mating CPAs through hinges. These combined
 527 assembly will be installed into the cryostat and the field cage module opens to bridge
 528 the CPA and the APA both mechanically and electrically.

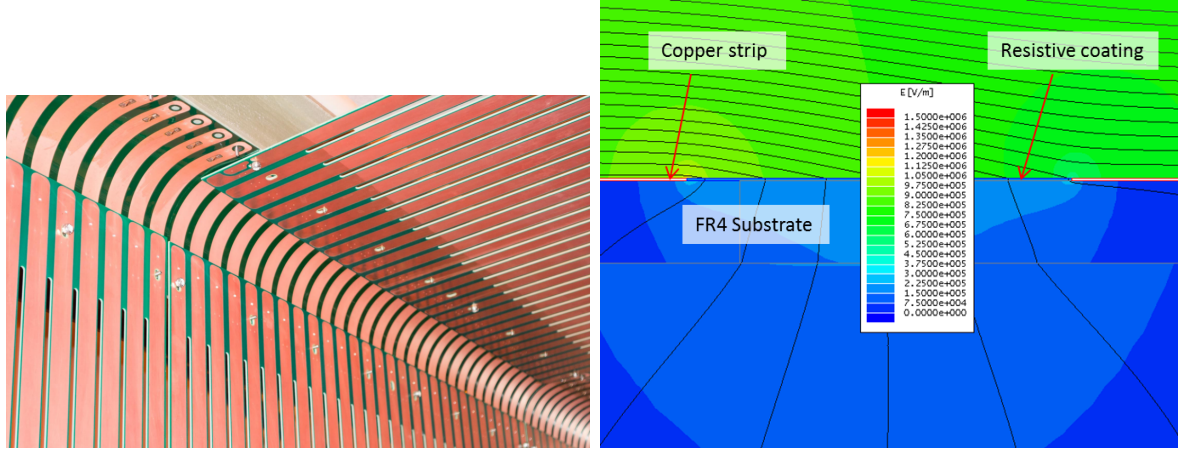


Figure 10: Left: A section of the field cage in the 35ton TPC. Right: Plot of electric field (color contours) and equi-potential contours (black lines) in a small region around the edges of two adjacent field cage strips on a 1.6mm thick FR4 substrate. A layer of resistive coating between the two copper strips nearly eliminated the high electric field regions at the copper edges

529 3.2.4 TPC Readout

530 The TPC electronics is designed to operate at liquid argon temperature and is placed as
 531 close to the sense wires as possible, thus minimizing the capacitance and the preamplifier
 532 noise. The present design has a maximum wire length of 7.3 m (induction planes) with
 533 a corresponding capacitance of 164 pF and an expected intrinsic noise of 400 electrons.
 534 The preamplifiers include shaping circuits, and are implemented in 16 channel front-end
 535 (FE) ASICs, which couple directly to 16 channel, 12 bit ADC ASICs operating at 2 MS/s,
 536 which include a 1:8 multiplexing stage. The ADCs are read out by a commercial FPGA,
 537 which provide an additional factor of 4 in multiplexing. This level of multiplexing is
 538 low enough for transmitting the entire raw data stream, while also being high enough
 539 that the number of signal lines is actually smaller than the number of the various power
 540 and control lines, and therefore easily manageable by a small number of feedthroughs.
 541 Neither zero suppression nor data compression is implemented at the level of the cold
 542 readout electronics. Not only does this greatly simplify the cold electronics design, but
 543 it also automatically satisfies the requirement that the system be capable of such raw
 544 readout, and further eliminates an entire class of failure-modes. The FPGAs transmit
 545 the data via high-speed (1 Gbps) serial links to the DAQ system. For the final detector
 546 it is expected that a dedicated digital control and data transmission ASIC (COLDATA)
 547 will be developed which replaces the commercial FPGA. While the COLDATA is well
 548 under way, it is not expected to be available in time for the CERN test, which will
 549 instead make use of the proven FPGA technology. While serious doubts regarding the
 550 longevity of commercially-available FPGAs at LAr temperatures strongly argues against
 551 their use in the Far Detector, where reliability over 15-20 years is required, this is not a
 552 concern for the CERN test, where the proven FPGA lifetime of at least a year is more
 553 than adequate.

554 The front end electronics is organized as a stack of three boards comprising the Cold

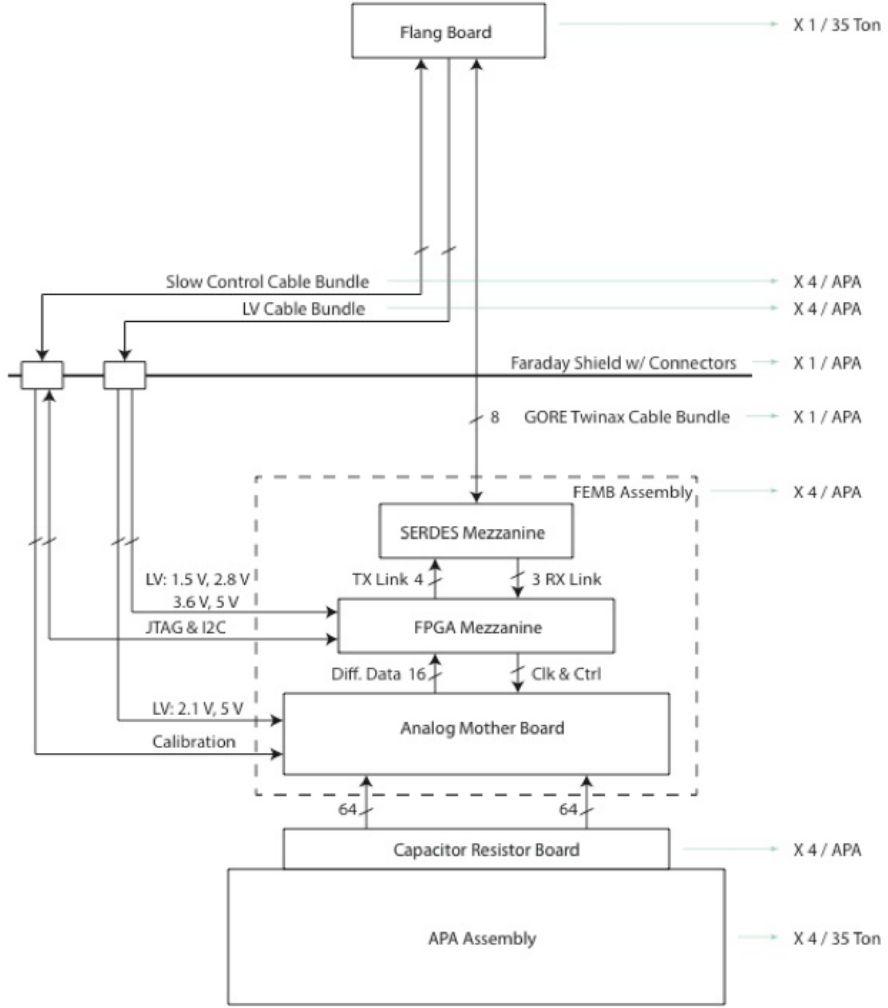


Figure 11: Layout of the TPC cold front-end (FE) electronics..

555 Mother Board assembly (CMB), which mounts directly on the APA. First is the Analog
 556 Mother Board, on which are mounted the FE and ADC ASICs. Second and third
 557 are the FPGA and SERDES Mezzanine Boards, themselves mounted on the Analog
 558 Mother Board. Each CMB has eight sets of FE and ADC ASICs and instruments 128
 559 wires. A Faraday cage (FC) covers the end of the APAs to shield the electronics from
 560 ambient noise. The FC also serves to prevent any Ar gas-bubbles from LAr boiled by
 561 the electronics' heat from entering the active TPC volume. Figure 11 shows a schematic
 562 of the cold electronics.

563 Besides the high-speed signal cable, which is a twin-axial cable bundle manufac-
 564 tured by GORE, there are cable bundles for low-voltage power, wire-bias voltages, and
 565 various slow controls and monitoring. The cable bundles will be connected through a
 566 feedthrough on the roof of the cryostat.

567 The primary interface between the TPC front-end electronics (FE) and the DAQ sub-
 568 system consists of an ATCA-based system of RCEs (Reconfigurable Cluster Elements).
 569 The RCE system receives the serialized raw data for the FE, performs zero-suppression

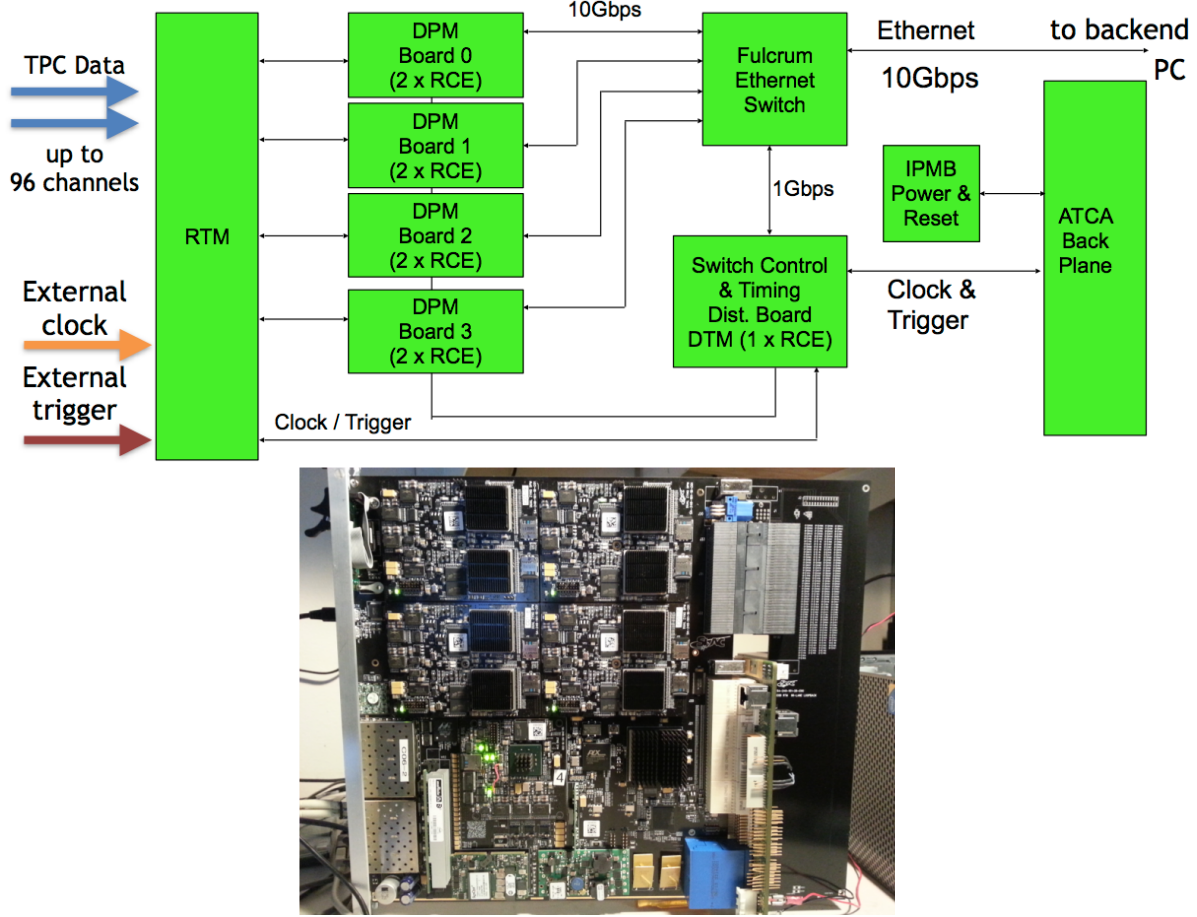


Figure 12: Top: Schematic for the TPC DAQ system. Bottom: The COB (left of the large connectors) and RTM (right).

570 on it, and packetizes and transmits the resulting sparsified data to a back-end data farm
 571 for event building and further processing. Additionally, the RCE system transmits tim-
 572 ing and control signals to the FE as well as forwarding configuration data to them at
 573 start-up.

574 The RCE system consists the following components: a commercial ATCA shelf (2-,
 575 6-, or 14-slot), a Cluster-On-Board (COB) which is the "front board" in ATCA terms,
 576 and a Rear-Transition-Module (RTM) which is the "rear board". A schematic of the
 577 system is shown in Figure 12. The COB is a custom board, developed by SLAC, which
 578 holds the processing power of the system. The COB (see Figure 12) consists of 5 bays for
 579 holding daughter boards, an onboard 10-GbE switch, and both 10- and 1-Gb ethernet
 580 connections for communications with the back-end system. Four of the daughter-board
 581 bays are for Data Processing Modules (DPM), each of which can hold up to two RCEs.
 582 The RCE is the core procession unit of the system; it is made up of a modern SoC
 583 (currently, the Xilinx Zynq-7045) with multiple high-speed I/O ports (up to 10-Gbps
 584 each) and external DRAM and flash memory controllers. The other bay on the COB
 585 contains the Data Transmission Module (DTM) which is responsible for distributing
 586 timing and trigger information to and between the DPMs.

587 While the COB hardware is application agnostic, the RTM is application specific.

588 The RTM provides the mechanical interface between the front-end (or, in our case, the
589 flange electronics) and the back-end, as well as other external sources such as the timing
590 or trigger systems. In this case we will use fiber optic connections between the flange
591 and the TPC DAQ using 8 12-channel (full duplex) CXP connectors on the RTM.

592 With the assumption that each cold FE board multiplexes it's 128 wire channels to 4
593 outputs at 1-Gbps each, the non-zero suppressed data for 1 APA can be fed into a single
594 COB (containing 8 RCEs). Each RCE would receive data from 2 FE boards, perform
595 zero-suppression, and send the result to the back-end.

596 3.2.5 Photon Detection System

597 The ELBNF far detector will utilize liquid argon scintillation light to determine the
598 prompt event time of beam-driven and non-beam events. While the TPC will have far
599 superior spatial resolution to a photon detection system, the drift time for TPC events
600 is on the order of milliseconds. The beam clock will give much better timing resolution
601 than this but a photon detection system can determine the start of an event occurring
602 in the TPC volume (or entering the volume) to about 6 ns, which will be useful in
603 determining the t_0 of cosmic ray events, events from radiological decays, and corrections
604 to energy loss of the drifting electrons.

605 A charged particle passing through liquid argon will produce about 40,000 128 nm
606 photons per MeV of deposited energy. At higher fields this will be reduced due to
607 reduced recombination, but at 500 V/cm the yield is still about 20,000 photons per
608 MeV. Roughly 1/3 of the photons are prompt 2-6 ns and 2/3 are generated with a
609 delay of 1100-1600 ns. LAr is highly transparent to the 128 nm VUV photons with a
610 Rayleigh scattering length and absorption length of 95 cm and >200 cm respectively.
611 The relatively large light yield makes the scintillation process an excellent candidate for
612 determination of t_0 for non-beam related events. Detection of the scintillation light may
613 also be helpful in background rejection.

614 Several prototypes of photon detection systems have been developed by the LBNE,
615 now ELBNF, photon detector group over the past few years. There are currently three
616 prototypes under consideration for use in the ELBNF far detector, a baseline design
617 along with two alternate designs. A decision on the design to be deployed in the CERN
618 test will be made in late 2015. The CERN neutrino platform ELBNF test would provide
619 the first full scale test of the ELBNF photon detector fully integrated into a full scale
620 TPC anode plane assembly.

621 The present reference design for the photon detection system is based on acrylic bars
622 that are 200 cm long and 7.63 cm wide, which are coated with a layer of tetraphenyl-
623 butadiene (TPB). The wavelength shifter converts VUV (128 nm) scintillation photons
624 striking it to 430 nm photons inside the bar, with an efficiency of 50% of converting
625 a VUV to an optical photon. A fraction of the wavelength-shifted optical photons are
626 internally reflected to the bar's end where they are detected by SiPMs whose QE is well
627 matched to the 430 nm wavelength-shifted photons. All PD prototypes are currently
628 using SensL MicroFB-6K-35-SMT 6 mm ? 6 mm devices.

629 A full 6 m long APA will be divided into 5 bays with 2 PD modules (paddles)
630 instrumenting each bay. The paddles will be inserted into the frames after the TPC
631 wires have been wrapped around the frames allowing final assembly at the CERN test

632 location. Two alternative designs are also under consideration.

633 One alternate design targeted increasing the geometrical acceptance of the photon de-
634 tectors by using large acrylic TPB coated plates with imbedded WLS fibers for readout.
635 In this design the number of required SiPMs and readout channels per unit detector area
636 covered with photon detection panels would be significantly reduced to keep the overall
637 cost for the photon detection system at or below the present design while increasing
638 the geometrical acceptance at the same time. The prototype consists of a TPB-coated
639 acrylic panel embedded with an S-shaped wavelength shifting (WLS) fiber. The fiber
640 is read out by two SiPMs, which are coupled to either end of the fiber and serves to
641 transport the light over long distances with minimal attenuation. The double-ended
642 fiber readout has the added benefit to provide some position dependence to the light
643 generation along the panel by comparing relative signal sizes and arrival times in the
644 two SiPMs.

645 The third design under consideration was motivated by increasing the attenuation
646 length of the PD paddles and allowing collection of 400 nm photons coming from any-
647 where in the active volume of the TPC. The fiber-bundle design is based on a thin TPB
648 coated acrylic radiator located in front of a close packed array of WLS fibers. This
649 concept is designed so that roughly half of the photons converted in the radiator are
650 incident on the bundle of fibers, the wavelength shifting fibers are Y11 UV/blue with
651 a 4% capture probability. The fibers are then read out using SiPMs at one end. The
652 Y11 Kuraray fibers have mean absorption and emission wavelengths of about 440 nm
653 and 480 nm respectively. The attenuation length of the Y11 fibers is given to be greater
654 than 3.5 m at the mean emission wavelength, which will allow production of full-scale
655 (2 m length) photon detector paddles.

656 The PD system tested at the CERN neutrino platform will be based on technology
657 selected later this year. The technology selection process will be based on a series of
658 tests planned for the next 6 months utilizing large research cryostats at Fermilab and
659 Colorado State University. The primary metric used for comparison between the three
660 technologies will be photon yield per unit cost. In addition to this metric PD threshold
661 and reliability will also serve as inputs to the final decision. A technical panel will be
662 assembled to make an unbiased decision.

663 Once the technology has been chosen the PD group will focus on optimizing the
664 selected design with the goal of procurement and assembly taking place in late FY 2016
665 and early FY 2016. The photon detector paddles will then be tested and shipped to
666 CERN in early FY 2017 for installation into the APAs in late FY 2017 in preparation
667 for installation into the test cryostat and operation in 2018.

668 3.2.6 DAQ, Slow control and monitoring

669 The DAQ will merge data to form events from the LArTPC, photon detector and beam
670 detector readouts using the artDAQ data acquisition toolkit using a farm of commercial
671 computers connected with an Ethernet switch. ArtDAQ is in use on several experiments
672 at Fermilab. We are using it on the 35t prototype, so we will have considerable experience
673 by the time of the CERN test.

674 The data collection for the CERN test will operate in a mode similar to that foreseen
675 for the underground detectors. In order to collect data from non-beam interactions such

as proton decay candidates or atmospheric neutrinos, data will be continuously read in to the artDAQ data receiver nodes and processed through the artDAQ system in quanta corresponding to time intervals fixed from the time of the beginning of the run. These are then transferred through the switch to a set of event building nodes which work in parallel, each node receiving all the data from all the detectors for the time intervals it is responsible for processing. There will be 32 parallel incoming data streams from the LArTPCs and 16 streams from the photon detectors. There will be an additional stream from the trigger board (the same board as built by Penn for the 35t test will be used) which will receive input of the spill gate, warning of extraction, and pattern-unit bits from trigger counters and other beamline instrumentation such as Cerenkov counters [Which section are these described in?, should we refer to them from here?].

Synchronisation across all the input sources is essential in order that artDAQ can bring together the data from the input streams correctly for processing by the event building nodes. The data receiver nodes will provide overlap by repeating the data at the boundaries of the time intervals so that a particle whose data spans two time intervals can be collected. The time synchronisation is provided to the RTM back-module on the LArTPC readout crates, to the SSP photon detector readout and to the trigger board from a GPS based time synchronisation distribution system originally designed for the NOvA experiment. This system includes functionality to calibrate and correct for the cable delays, and to send synchronisation control signals to the readout at predetermined times.

The event building nodes will select time regions of interest within the time intervals they are processing and form these into events to be written to disk. The algorithms to select the events may be as simple as looking for a trigger bit in the trigger board data stream, or may involve looking for self-triggered events in the LArTPC data. An aggregation task, which is part of artDAQ will handle the parallelized event building processes by merging the output events into a single stream and writing them to disk. To avoid oversized output data files, when a predetermined file size is reached, the aggregator will switch to writing to a new file. The collaboration requests to CERN, data links of sufficient bandwidth to transfer these files from the CENF to the CERN data center, and from there to locations worldwide for analysis.

Improved versions of the software systems which are being prototyped at the 35t test will available for the CERN test including (a) Run control which controls and monitors the DAQ processes and allows run starts and stops to be performed by the operator (b) online monitoring (c) slow control of voltages and temperatures being used by the electronics (this may not be comprehensive by the time of the CERN prototype, but we plan on prototyping the readout of some of the quantities). The trigger board includes facilities for generating calibration pulses and for identifying the event times of the calibration events.

3.2.7 Installation

The interior of the cryostat will be prepared prior to the installation of the TPC. A series of support rails will be suspended below the top surface of the cryostat membrane. These will be structurally supported by a truss structure above the cryostat. These supports will pass through the top of the cryostat. They need to be designed to minimize the heat

720 gain into the cryogenic volume. For the CPAs, the rails need to be electrically isolated
721 due to high voltage concerns. To preserve the ability to reverse the order of the TPC
722 components, all of the support rails will be designed to the same set of requirements
723 regarding loads and attachment points.

724 There will be a series of feed thru flanges located along each of the support rails.
725 These will be cryogenic flanges where the services for the TPC components can pass
726 through the top of the cryostat. It is foreseen that each CPA will require one feed thru
727 for the high voltage probe to bring in the drift voltage. The drift voltage is 500 V/cm.
728 For a drift distance of 2.5 m, the probe voltage will be 125 kV. There will be one service
729 feed thru for each of the APAs. These feed thrus will include high speed data, bias
730 voltages for the wire planes, control and power for the cold electronics.

731 The main TPC components will be installed through a large hatch in the top of the
732 cryostat. This is similar to the installation method intended for the detector at the far
733 site. This hatch will have an aperture approximately 2.0 m wide and 3.5 m long. Each
734 APA and CPA panel will be carefully tested after transport into the clean area and
735 before installation into one of the cryostats. Immediately after a panel is installed it will
736 be rechecked. The serial installation of the APAs along the rails means that removing
737 and replacing one of the early panels in the row after others are installed would be very
738 costly in effort and time. Therefore, to minimize the risk of damage, as much work
739 around already installed panels as possible will be completed before proceeding with
740 further panels. The installation sequence is planned to proceed as follows:

- 741 1. Install the monorail or crane in the staging area outside the cryostat, near the
742 equipment hatch.
- 743 2. Install the relay racks on the top of the cryostat and load with the DAQ and power
744 supply crates.
- 745 3. Dress cables from the DAQ on the top of the cryostat to remote racks.
- 746 4. Construct the clean-room enclosure outside the cryostat hatch.
- 747 5. Install the raised-panel floor inside the cryostat.
- 748 6. Insert and assemble the stair tower and scaffolding in the cryostat.
- 749 7. Install the staging platform at the hatch entrance into the cryostat.
- 750 8. Install protection on (or remove) existing cryogenics instrumentation in the cryo-
751 stat.
- 752 9. Install the cryostat feedthroughs and dress cables inside the cryostat along the
753 support beams.
- 754 10. Install TPC panels:
 - 755 (a) Install both pairs of CPA panels. These will be installed from the floor of the
756 cryostat. Access to the top edge will be required by scaffolding.
 - 757 (b) Install and connect HV probe for each of the CPAs.

- (c) Perform electrical tests on the connectivity of the probe to the CPAs.
 - (d) Install first end wall of vertical field cage at the non-access end of the cryostat. These will be installed from the floor of the cryostat. Scaffolding will be needed to install the supporting structure and then attach the panels to the structure.
 - (e) Test the inner connections of the field cage panels.
 - (f) Install the first APA and connect to the far end field cage support.
 - (g) Connect power and signal cables. This will require scaffolding to access the top edge of the APA.
 - (h) Test each APA wire for expected electronics noise. Spot-check electronics noise while cryogenics equipment is operating.
 - (i) Install the upper field cage panels for the first APA between the APA and CPAs. This will require scaffolding to access the upper edge of the APA, CPA and field cage structure.
 - (j) Perform electrical tests on upper field cage panels.
 - (k) Repeat steps (f) through (j) for the next two APAs.
 - (l) Install the lower field cage panels between the APAs and CPAs. Start at the far end away from the access hatch and work towards the hatch.
 - (m) Perform electrical test on lower field cage panels and the entire loop around the TPC.
 - (n) Remove temporary floor sections as the TPC installation progresses.
 - (o) Install sections of argon-distribution piping as the TPC installation progresses.
 - (p) Install the final end wall of vertical field cage at the access end of the cryostat. These will be installed from the floor of the cryostat. Scaffolding will be needed to install the supporting structure and then attach the panels to the structure.

11. Remove movable scaffold and stair towers.
12. Temporarily seal the cryostat and test all channels for expected electronics noise.
13. Seal the access hatch.
14. Perform final test of all channels for expected electronics noise.

In general, APA panels will be installed in order starting with the panel furthest from the hatch side of the cryostat and progressing back towards the hatch. The upper field cage will be installed in stages as the installation of APA and CPAs progresses. After the APAs are attached to the support rods the electrical connections will be made to electrical cables that were already dressed to the support beams and electrical testing will begin. Periodic electrical testing will continue to assure that nothing gets damaged during the additional work around the installed APAs.

796 The TPC installation will be performed in three stages, each in a separate location;
797 the locations, or zones. First, in the clean room vestibule, a crew will move the APA
798 and CPA panels from storage racks, rotate to the vertical position and move them into
799 the cryostat. A second crew will transfer the lower panels from the crane to the staging
800 platform, where the crew inside the cryostat will connect the upper and lower panels
801 together, route cables to the top of stacked panels and finally transfer the stacked panels
802 on to the rails within the cryostat. A third crew will reposition the movable scaffolding
803 and use the scaffold to make the mechanical and electrical connections at the top for
804 each APA and CPA as they are moved into position.

805 The requirements for alignment and survey of the TPC are under development.
806 Since there are many cosmic rays in the surface detector and beam events, significant
807 corrections can be made for any misalignment of the TPC. The current plan includes
808 using a laser guide or optical transit and the adjustment features of the support rods
809 for the TPC to align the top edges of the APAs in the TPC to be straight, level and
810 parallel within a few mm. The alignment of the TPC in other dimensions will depend
811 on the internal connecting features of the TPC. The timing of the survey will depend
812 on understanding when during the installation process the hanging TPC elements are
813 in a dimensionally stable state. The required accuracy of the survey is not expected to
814 be more precise than a few mm.

815 **4 Cryostat and cryogenics system [~5 pages; David/Barry/Jack]**

816 **4.1 Cryostat**

817 The Single Phase TPC test at CERN will use a membrane tank technology to contain
818 725 tons of LAr, equivalent to about $520m^3$. The design is based on a scaled up version
819 of the LBNE 35-ton Prototype and the Fermilab Short-Baseline Near Detector. The
820 cryostat will use a steel outer supporting structure with a metal liner inside to isolate
821 the insulation volume, similar to the one of the dual phase detector prototype WA105
822 $1 \times 1 \times 3$ and to the Fermilab Short-Baseline Near Detector. The support structure
823 will rest on I-beams to allow for air circulation underneath in order to maintain the
824 temperature within the allowable limits. This section describes the proposed design,
825 whose scope encompasses the following components:

- 826 • steel outer supporting structure,
- 827 • main body of the membrane cryostat (sides and floor),
- 828 • top cap of the membrane cryostat.

829 A membrane cryostat design commonly used for liquefied natural gas (LNG) storage
830 and transportation will be used. In this vessel a stainless steel membrane contains
831 the liquid cryogen. The pressure loading of the liquid cryogen is transmitted through
832 rigid foam insulation to the surrounding outer support structure, which provides external
833 support. The membrane is corrugated to provide strain relief resulting from temperature
834 related expansion and contraction. The vessel is completed with a top cap that uses the
835 same technology.

836 Two membrane cryostat vendors are known: GTT (Gaztransport & Technigaz) from
837 France and IHI (Ishikawajima-Harima Heavy Industries) from Japan. Each one is tech-
838 nically capable of delivering a membrane cryostat that meets the design requirements
839 for this detector. To provide clarity, only one vendor is represented in this document,
840 GTT; this is for informational purposes only. Figure 1 shows a 3D model of the GTT
841 membrane and insulation design.

842 The conceptual proposed design for the Single Phase Test at CERN cryostat is a
843 rectangular vessel measuring 9.5 m in length (parallel to the beam direction), 7.3 m in
844 width, and 8.40 m in height; containing a total mass of 725 tons of liquid argon. Figure 15
845 shows side and end views of the cryostat respectively. Figure 3 shows a 3D view. To
846 minimize the contamination from warm surfaces, during operation the temperature of all
847 surfaces in the ullage shall be lower than 100 K. The top plate will contain two hatches,
848 one to install the TPCs and the other to access the tank; it will also contain a manhole
849 to enter the tank after closing the hatches, and several penetrations for the cryogenic
850 system and the detector.

851 **Design Parameters**

852 This design includes technical solutions that may be of interested for the future needs
853 of the Long Baseline Neutrino program. For example the use of a cold ullage (<100 K)
854 to lower the impurities in the gas region, and of a LAr pump outside the cryostat to
855 minimize the effect of noise, vibration and microphonics to the TPC inside the liquid
856 argon volume.

857 The design parameters for the TPC Test at CERN cryostat are listed in Table 4.

858 **Insulation system and secondary membrane**

859 The membrane cryostat requires insulation applied to all internal surfaces of the
860 outer support structure and roof in order to control the heat ingress and hence required
861 refrigeration heat load. To avoid bubbling of the liquid Argon inside the tank, the
862 maximum static heat leak is $10W/m^2$ for the floor and the sides and $15W/m^2$ for the
863 roof, higher to account for the penetrations that increase the heat budget. Preliminary
864 calculations show that these values it can be obtained using 0.9 m thick insulation
865 panels of polyurethane foam. Given an average thermal conductivity coefficient for the
866 insulation material of $0.0283\text{ W}/(\text{m}\cdot\text{K})$, the heat input from the surrounding steel is
867 expected to be about 3.4 kW total. It assumes that the hatches are foam insulated as
868 well. This is shown in Table 5.

869 The insulation material is a solid reinforced polyurethane foam manufactured as
870 composite panels. The panels get laid out in a grid with 3 cm gaps between them
871 (that will be filled with fiberglass) and fixed onto anchor bolts anchored to the support
872 structure. The composite panels contain the two layers of insulation with the secondary
873 barrier in between. After positioning adjacent composite panels and filling the 3-cm
874 gap, the secondary membrane is spliced together by epoxying an additional overlapping
875 layer of secondary membrane over the joint. All seams are covered so that the secondary
876 membrane is a continuous liner.

877 In the current GTT design, the secondary membrane is comprised of a thin aluminum
878 sheet and fiberglass cloth. The fiberglass-aluminum-fiberglass composite is very durable
879 and flexible with an overall thickness of about 1 mm. The secondary membrane is placed
880 within the insulation space. It surrounds the bottom and sides. In the unlikely event of
881 an internal leak from the primary membrane of the cryostat into the insulation space, it

GST® Containment System

AS A PRIMARY BARRIER :

a flexible (1.2mm) stainless steel membrane



The double network of corrugations absorbs the thermal contractions due to the very low temperature of the LNG.

Insulating panel

The thickness of the panels can be adjusted to provide a large range of boil-off rates according to the operator's requirements (typically 0.05% per day).

Plywood

Reinforced polyurethane foam

AS A SECONDARY BARRIER :

a composite laminated material

This consists of a thin sheet of aluminium between two layers of glass cloth and resin.

In the event of a failure of the primary membrane, it prevents the build-up of stress concentrations on concrete corner and ensures the liquid tightness of the concrete wall.

Reinforced polyurethane foam

Plywood

Mastic

Post-tensionned concrete covered by a moisture barrier

The outer concrete container provides the *structural resistance* to internal (LNG hydrostatic & dynamic pressure, and vapour gas pressure) and external (wind, snow, ice) loads.

A moisture barrier, applied on its inner side, prevents moisture from entering the tank.

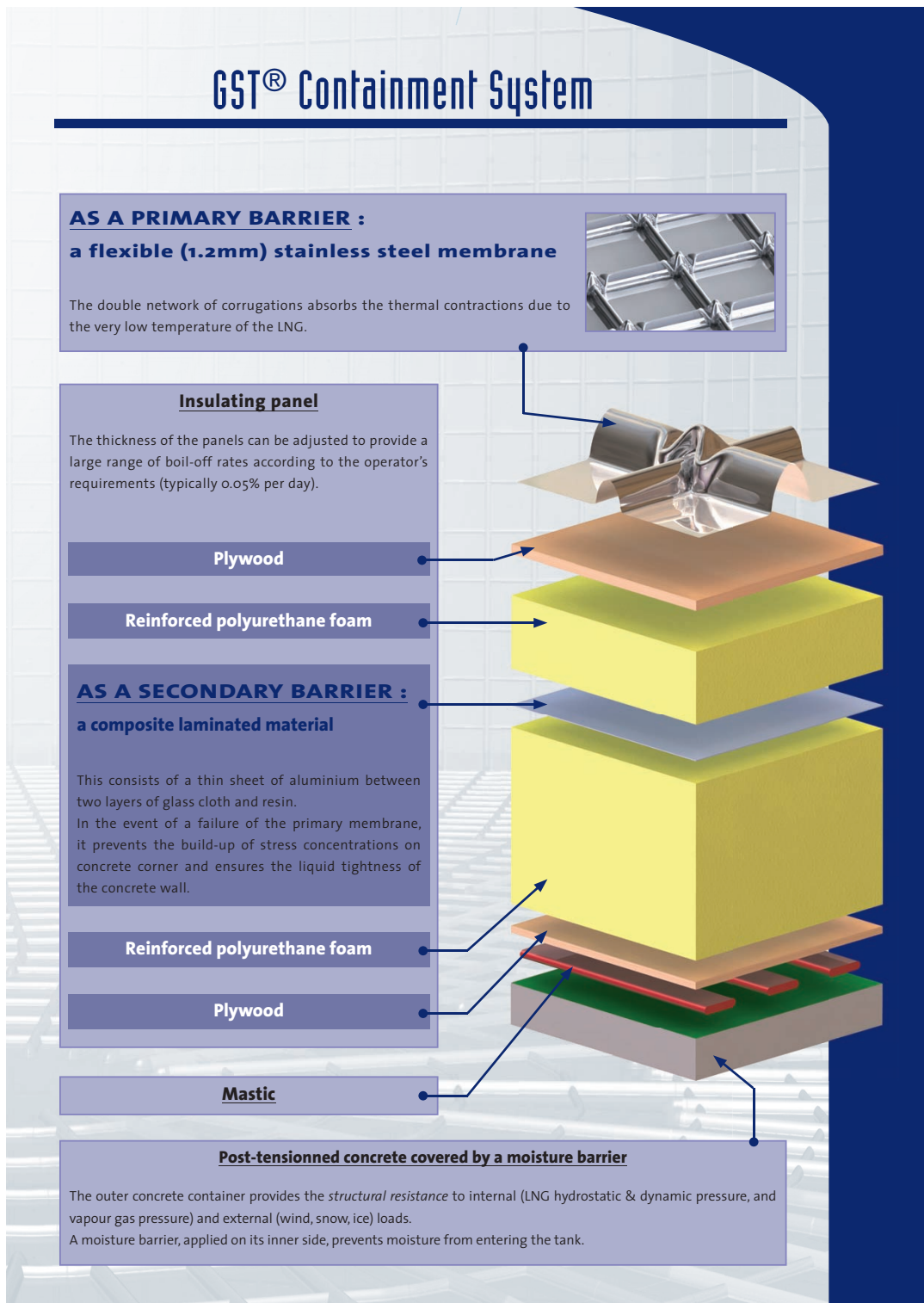


Figure 13: Exploded view of the membrane cryostat technology

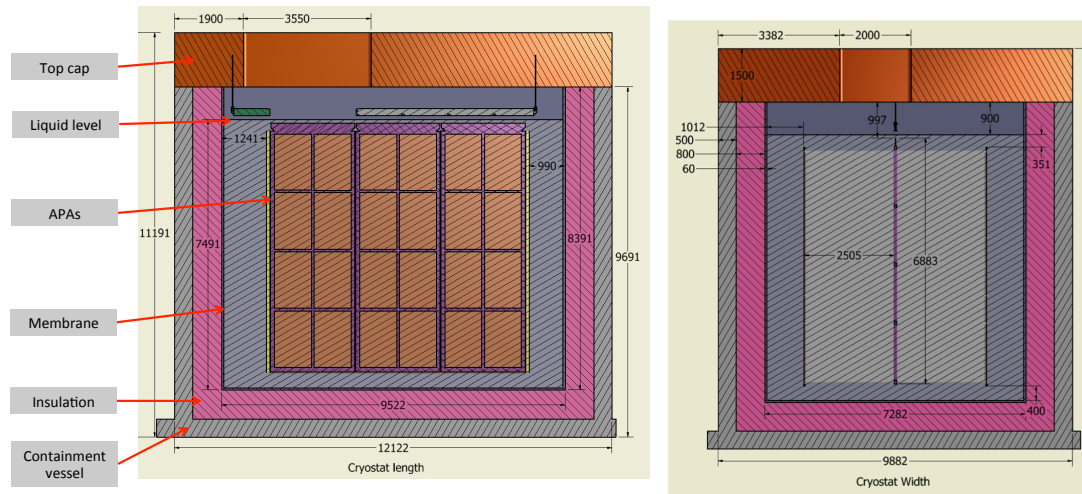


Figure 14: Side (left) and end (right) views of cryostat

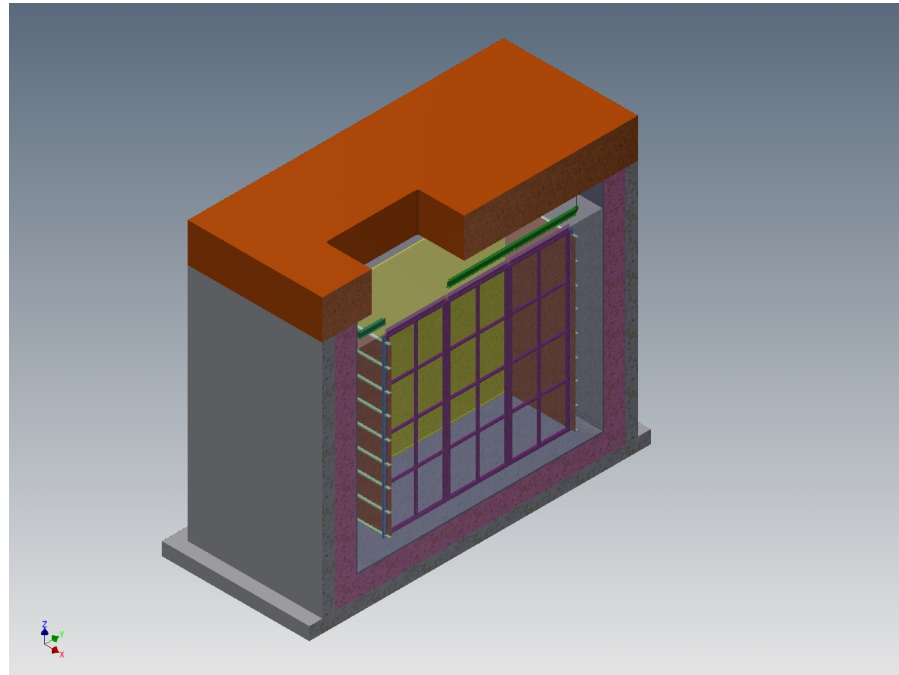


Figure 15: Isometric view of the membrane cryostat

Table 4: Design requirements for the membrane cryostat

| Design Parameter | Value |
|--|--|
| Type of structure | Membrane cryostat |
| Membrane material | SS 304/304L, 316/316L or equivalent. |
| Fluid | Liquid argon (LAr) |
| Other materials upon approval. | |
| Outside reinforcement (support structure) | Steel enclosure with metal liner to isolate the outside from the insulation space, standing on legs to allow for air circulation underneath. |
| Total cryostat volume | 583 m3 |
| Total LAr volume | 520 m3 |
| LAr total mass | 725,000 kg |
| Minimum inner dimensions (flat plate to flat plate). | 7.3 m (W) x 9.5 m (L) x 8.4 m (H) |
| Depth of LAr | 7.5 m (0.9 m ullage, same as LBNF) |
| Primary membrane | 1.2 mm thick SS 304L corrugated stainless steel |
| Secondary barrier system | GTT design; 0.07 mm thick aluminum between fiberglass cloth. Overall thickness 1 mm located between insulation layers. |
| Insulation | Polyurethane foam (0.9 m thick from preliminary calculations) |
| Maximum static heat leak | 10 W/m2 |
| LAr temperature | 88 +/- 1K |
| Operating gas pressure | Positive pressure. Nominally 70 mbarg (~1 psig) |
| Vacuum | No vacuum |
| Design pressure | 350 mbarg (~5 psig) + LAr head (1,025 mbarg) |
| Design temperature | 77 K (liquid nitrogen temperature for flexibility) |
| Temperature of all surfaces in the ullage during operation | <100 K |
| Leak tightness | $1e - 6$ mbar*l/sec |
| Maximum noise/vibration/microphonics inside the cryostat | LAr pump outside the cryostat |
| Beam window | Precise location TBD. Figure 15 shows the location where the beam enters the cryostat. |
| Accessibility after operations | Capability to empty the cryostat in 30 days and access it in 60 days after the end of operations. |
| Lifetime / Thermal cycles | Consistent with liquid argon program. TBD. |

882 will prevent the liquid cryogen from migrating all the way through to the steel support
 883 structure where it would degrade the insulation thermal performance and could possibly
 884 cause excessive thermal stress in the support structure. The liquid cryogen, in case of
 885 leakage through the inner (primary) membrane will escape to the insulation volume,
 886 which is purged with GAr at the rate of one volume exchange per day.

Table 5: Heat load calculation for the membrane cryostat (insulation thickness = 0.9 m). (note to self: has right values)

| Element | Area (m^2) | K (W/mK) | $\Delta T (K)$ | Heat Input (W) |
|----------------|--------------------------------|-----------------|----------------------------------|-----------------------|
| Base | 83 | 0.0283 | 205 | 550 |
| End walls | 190 | 0.0283 | 205 | 1,247 |
| Side walls | 149 | 0.0283 | 205 | 983 |
| Roof | 83 | 0.0283 | 205 | 550 |
| | | | | |
| Total | | | | 3,330 |

Cryostat Configuration

887 With the intent to minimize the contamination in the gas region, the ullage will be
 888 kept cold (<100 K). It has been observed in the Materials Test Stand (MTS) and the
 889 Liquid Argon Purity Demonstrator (LAPD) at Fermilab that the outgassing is signifi-
 890 cantly reduced below 100 K [add reference]. A possible way to achieve this requirement
 891 is to spray a mist of clean liquid and gaseous argon to the metal surfaces in the ullage
 892 and keep them cold, similar to the strategy that was developed for the cool down of the
 893 LBNE 35 Ton prototype.

Outer Support Structure

894 The proposed design is a steel support structure with a metal liner on the inside
 895 to isolate the insulation region and keep the moisture out. This choice allows natural
 896 and forced ventilation to maintain the temperature of the steel within its limit, without
 897 the need of heating elements and temperature sensors. It reduces the time needed for
 898 the construction: the structure will be prefabricated in pieces of dimensions appropriate
 899 for transportation, shipped to the destination and only assembled in place. Fabrication
 900 will take place at the vendor's facility for the most part. This shortens the construction
 901 of the outer structure on the detector site, leaving more time for completion of the
 902 building infrastructure. If properly designed, a steel structure may allow the cryostat to
 903 be moved, should that be desired in the future.

Main body of the membrane cryostat

904 The sides and bottom of the vessel constitute the main body of the membrane cryo-
 905 stat. They consist of several layers. From the inside to the outside the layers are stainless
 906 steel primary membrane, insulation, thin aluminum secondary membrane, more insula-
 907 tion, and steel outer support structure with metal panels acting as vapor barrier. The
 908 secondary membrane contains the LAr in case of any primary membrane leaks and
 909 the vapor barrier prevents water ingress into the insulation. The main body does not
 910 have side openings for construction. The access is only from the top. There is a side
 911 penetration for the liquid argon pump for the purification of the cryogen.

915 **Top cap**

916 Several steel reinforced plates welded together constitute the top cap. The stainless
917 steel primary membrane, intermediate insulation layers and vapor barrier continue across
918 the top of the detector, providing a leak tight seal. The secondary barrier is not used
919 nor required at the top. The cryostat roof is a removable steel truss structure that also
920 supports the detector. Stiffened steel plates are welded to the underside of the truss to
921 form a flat vapor barrier surface onto which the roof insulation attaches directly. The
922 penetrations will be clustered in the back region. The top cap will have a large opening
923 for TPC installation, a secondary smaller opening for personnel access and a manhole
924 to enter the tank after the hatches have been closed.

925 The truss structure rests on the top of the supporting structure where a positive
926 structural connection between the two is made to resist the upward force caused by the
927 slightly pressurized argon in the ullage space. The hydrostatic load of the LAr in the
928 cryostat is carried by the floor and the sidewalls. Everything else within the cryostat
929 (TPC planes, electronics, sensors, cryogenic and gas plumbing connections) is supported
930 by the steel plates under the truss structure. All piping and electrical penetration into
931 the interior of the cryostat are made through this top plate, primarily in the region of
932 the penetrations to minimize the potential for leaks. Studs are welded to the underside
933 of the top plate to bolt the insulation panels. Insulation plugs are inserted into the
934 bolt-access holes after panels are mounted. The primary membrane panels are first
935 tack-welded then fully welded to complete the inner cryostat volume.

936 Table 6 presents the list of the design parameters for the top of the cryostat.

937 **Cryostat grounding and isolation requirements**

938 The cryostat has to be grounded and electrically isolated from the building. This
939 section presents the list of the current grounding and isolation requirements for the
940 cryostat. Figure 16 shows the layout of the top plate grounding.

941 **Isolation**

- 942 1. The cryostat membrane and any supporting structure, whether it is a steel struc-
943 ture or a concrete and rebar pour, shall be isolated from any building metal or
944 building rebar with a DC impedance greater than $300\text{ k}\Omega$.
- 945 2. All conductive piping penetrations through the cryostat shall have dielectric breaks
946 prior to entering the cryostat and the top plate.

947 **Grounding**

- 948 1. The cryostat, or “detector” ground, shall be separated from the “building” ground.
- 949 2. A safety ground network consisting of saturated inductors shall be used between
950 detector ground and building ground.
- 951 3. Parameters TBD.

952 **Top plate grounding**

- 953 1. If the cryostat is contained within a concrete pour, the top plate shall be electrically
954 connected to any rebar used in that pour, and the rebar shall be conductively tied
955 at regular intervals. Parameters TBD.

Table 6: Design parameters for the top of the cryostat

| Design Parameter | Value |
|---|---|
| Configuration | Removable metal plate reinforced with trusses/I-beams anchored to the membrane cryostat support structure. Contains multiple penetrations of various sizes and a man-hole. Number, location and size of the penetrations TBD. Provisions shall be made to allow for removal and re-welding six (6) times. |
| Plate/Trusses non-wet material | Steel if room temperature. SS 304/304 or equivalent if at cryogenic temperature |
| Wet material | SS 304/304L, 316/316L or equivalent. Other materials upon approval. |
| Fluid | Liquid argon (LAr) |
| Design pressure | 350 mbarg (5 psig) |
| Design temperature | 77 K (liquid nitrogen temperature for flexibility) |
| Inner dimensions | To match the cryostat |
| Maximum allowable roof deflection | 0.028 m (span/360 from LBNF) |
| Maximum static heat leak | <15 W/m ² |
| Temperatures of all surfaces in the ullage during operation | <100 K |
| Additional design loads | <ul style="list-style-type: none"> - Top self-weight - TPC (3,000 kg on each anchor) - TPC anchors (TBD) - Live load (488 kg/m²) - Electronics racks (400 kg in the vicinity of the feed through) - Services (150 kg on every feed through) |
| TPC anchors | Capacity: 3,000 kg each anchor. Number and location TBD. Minimum 6. |
| Hatch opening for TPC installation | 3,550 m x 2,000 m (location TBD) |
| Grounding plate | 1.6 mm thick copper sheet brazed to the bottom of the top plate |
| Lifting fixtures | Appropriate for positioning the top at the different parts that constitute it. |
| Cold penetrations | Location and design TBD. |
| Lifetime / Thermal cycles | Consistent with the liquid argon program TBD. |

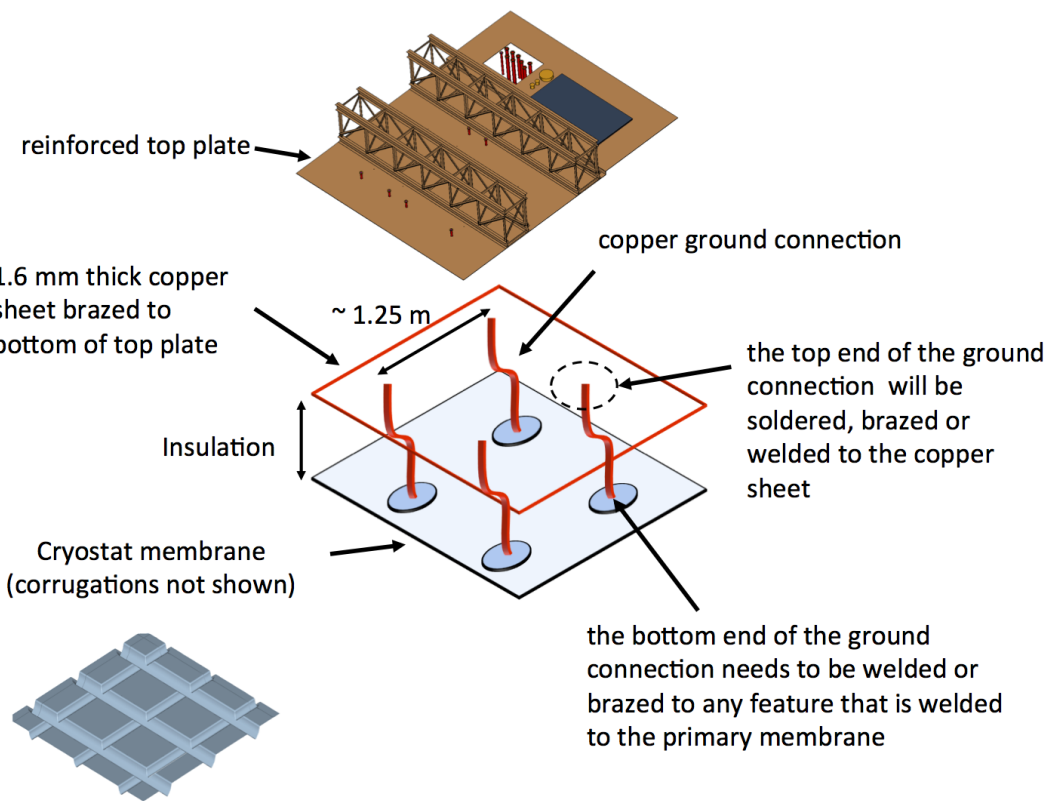


Figure 16: Top plate grounding layout

- 956 2. The top grounding plate shall be electrically connected to the cryostat membrane
 957 by means of copper braid connections.
- 958 (a) Each connection shall be at least 1.6 mm thick and 63.5 mm wide.
 959 (b) The length of each connection is required to be as short as possible.
 960 (c) The distance between one connection and the next one shall be no more than
 961 1.25 m.
 962 (d) The layout can follow the profile of several pieces of insulation, but it shall
 963 be continuous.
 964 (e) The DC impedance of the membrane to the top plate shall be less than 1
 965 ohm.

966 **Leak prevention**

967 The primary membrane will be subjected to several leak tests and weld remediation,
 968 as necessary. All (100%) of the welds will be tested by an Ammonia colorimetric leak
 969 test (ASTM E1066-95) in which welds are painted with a reactive yellow paint before
 970 injecting a Nitrogen-Ammonia mixture into the insulation space of the tank. Wherever
 971 the paint turns purple or blue, a leak is present. The developer is removed, the weld
 972 fixed and the test is performed another time. Any and all leaks will be repaired. The

973 test lasts a minimum of 20 hours and is sensitive enough to detect defects down to
974 0.003 mm in size and to a $10^{-7} \text{ std} - \text{cm}^3/\text{s}$ leak rate (equivalent leak rate at standard
975 pressure and temperature, 1 bar and 273 K). To prevent infiltration of water vapor
976 or oxygen through microscopic membrane leaks (below detection level) the insulation
977 spaces will be continuously purged with gaseous argon to provide one volume exchange
978 per day. The insulation space will be maintained at 70 mbar, slightly above atmospheric
979 pressure. This space will be monitored for changes that might indicate a leak from the
980 primary membrane. Pressure control devices and safety relief valves will be installed on
981 the insulation space to ensure that the pressure does not exceed the operating pressure
982 inside the tank. The purge gas will be recirculated by a blower, purified, and reused as
983 purge gas. The purge system is not safety- critical; an outage of the purge blower would
984 have negligible impact on LAr purity.

985 4.2 Cryostat size from TPC dimensions (Move to begining of 986 sec 4 per DM)

987 The minimum internal size of the cryostat is determined from size of the TPC. At the
988 bottom of the cryostat there needs to be a minimum of 0.3 m between the frame of the
989 CPA and closest point on the SS membrane. This is to prevent high voltage discharge
990 between the CPA and the electrically grounded membrane. It is foreseen that there
991 would be some cryogenic piping and instrumentation under the TPC. There is a height
992 allowance of 0.1 m for this. There will be access and egress space around the outside of
993 the TPC and the membrane walls. On three sides, 1.0 m of space is reserved for this.
994 The final side of the TPC will have piping and instrumentation for the cryogenic system.
995 There will be 1.3 m of space reserved for this.

996 The support system for the TPC will be located at the top between the underside
997 of the cryostat roof and the top of the TPC. The plan is to model this space similar to
998 what is planned for the far site TPC. There will be 0.9 m of ullage space. In order to
999 prevent high voltage discharge, the upper most part of the CPA needs to be submerged a
1000 minimum of 0.3 m below the liquid Argon surface. The top of the TPC will be separated
1001 from the membrane by a minimum of 1.2 m.

1002 Adding all of these to the size of the TPC yields the minimum inner dimensions of
1003 the cryostat. A minimally sized cryostat would be 9.5 m long, 7.3 m wide and 8.4 m
1004 high. This assumes the TPC will be positioned inside the cryostat with the CPAs and
1005 end field cages parallel to the walls of the cryostat. Also there is no space allotted for
1006 a beam window to enter the cryostat. Clearance would need to be added if it violates
1007 any of the current boundaries listed above. These dimensions also preserve the ability
1008 to reverse the order of the APAs and CPAs inside the TPC. The current plan is to have
1009 the APAs located in the center of the cryostat with a CPA on each side. Reversing this
1010 to have the CPA in the center and APAs on each side may be required to achieve some
1011 of the proposed physics. The orientation of the TPC components will be finalized after
1012 various scenarios have been sufficiently simulated.

1013 **4.3 Cryogenic System**

1014 Figure 17 outlines the basic scheme of the LN2 supply system, which was proposed
1015 by CERN for the Short Baseline Program and found to be an appropriate solution for
1016 this detector as well. The experiment will rely on LN2 tankers for regular deliveries to a
1017 local dewar storage, which will be sized to provide several days of cooling capacity in the
1018 event of a delivery interruption. From the dewar storage the LN2 is then transferred to
1019 a distribution facility located in the experimental hall. It includes a small buffer volume
1020 and an LN2 pumping station that transfers the LN2 to the argon condenser and other
1021 services as needed. The low estimated heat leak of the vessel (~ 3.4 kW) and the location
1022 inside an above ground building allow for use of an open loop system typical of other
1023 installations operated at Fermilab (LAPD, LBNE 35 ton prototype, MicroBooNE) and
1024 at CERN (???). Main goal of the LN2 system is to provide cooling power for the argon
1025 condenser, the initial cool down of the vessel and the detector, and all other services as
1026 needed.

1027 Table 7 presents the list of requirements for the cryogenic system for the Single Phase
1028 TPC test at CERN detector.

1029 Figure 18 shows a schematic diagram of the proposed liquid argon system. It is based
1030 on the design of the LBNE 35 ton prototype, the MicroBooNE detector systems and the
1031 current plans for the Long Baseline Far Detector.

1032 Main goal of the LAr system is to purge the cryostat prior to the start of the opera-
1033 tions (with GAr in open and closed loop), cool down the cryostat and fill it with LAr.
1034 Then continuously purify the LAr and the boil off GAr to maintain the required purity
1035 (electron lifetime measured by the detector).

1036 The LAr receiving facility includes a storage dewar and an ambient vaporizer to
1037 deliver LAr and GAr to the cryostat. The LAr goes through the liquid argon handling
1038 and purification system, whereas the Gar through the gaseous argon purification before
1039 entering the vessel.

1040 The LAr purification system is currently equipped with a filter containing mol sieve
1041 and copper beds, and a regeneration loop to regenerate the filter itself. Filters containing
1042 Oxsorb and Hydrosorb rather than mol sieve and copper beds, were also successfully
1043 employed. Same concept, but different medium. Studies are ongoing to standardize the
1044 filtration scheme and select the optimal filter medium for all future generation detectors,
1045 including this test prototype.

1046 During operation, an external LAr pump circulates the bulk of the cryogen through
1047 the LAr purification system. The boil off gas is first recondensed and then is sent to the
1048 LAr purification system before re- entering the vessel.

Table 7: Design requirements for the cryogenic system

| Parameter | Value |
|---|--|
| Location | Preferably not in front of the cryostat (on the beam) |
| Cooling Power | TBD based on the heat leak of the cryostat (estimated 3.4 kW), the cryo-piping and all other contributions (cryogenic pumps, etc.) |
| Liquid argon purity in cryostat | 10 ms electron lifetime (30 ppt O ₂ equivalent) |
| Gaseous argon piston purge rate of rise | 1.2 m/hr |
| Membrane cool-down rate | From manufacturer |
| TPCs cool-down rate | <40 K/hr, <10 K/m (vertically) |
| Mechanical load on TPC | The LAr or the gas pressure shall not apply a mechanical load to the TPC greater than 200 Pascal. |
| Nominal LAr purification flow rate (filling/ops) | 5.5 day/volume exchange |
| Temperature of all surfaces in the ullage during operations | <100 K |
| Gaseous argon purge within insulation | 1 volume change /day of the open space between insulation panels. |
| Lifetime of the cryogenic system | Consistent with the LAr program. TBD. |

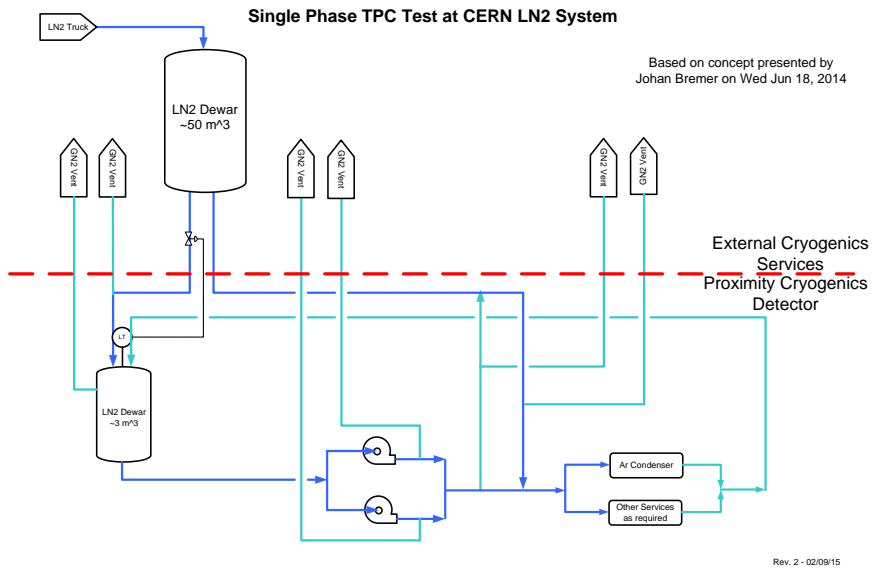


Figure 17: Schematic diagram for the proposed LN2 system

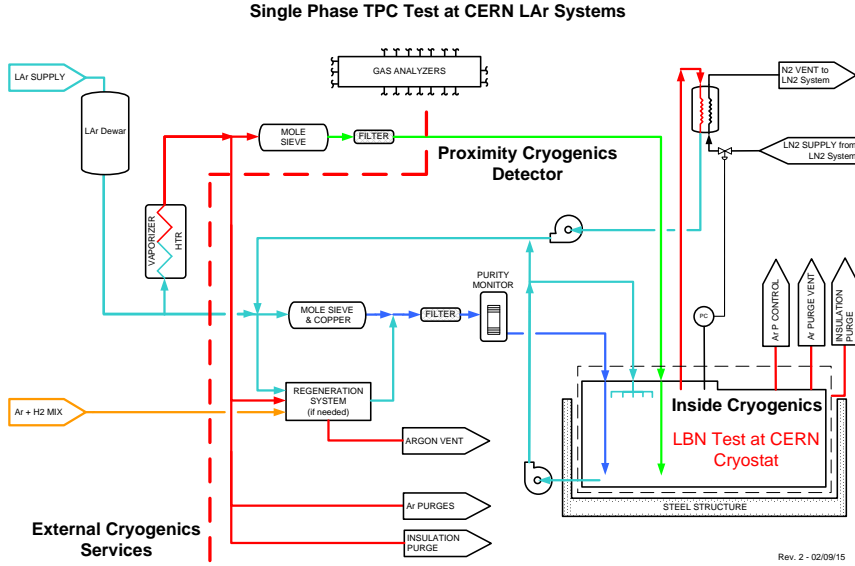


Figure 18: Schematic diagram for the proposed LAr system

1049 5 Charged Particle Test Beam Requirements [~ 10 1050 pages; Cheng-Ju]

1051 5.1 Particle Beam Requirements

1052 The requested beam parameters are driven by the requirement that the results from the
 1053 CERN test beam should be directly applicable to the future large underground single-
 1054 phase LAr detector with minimal extrapolation. The CERN test beam data will be
 1055 used to evaluate the detector performance, to understand the various physics systematic
 1056 effects, and to provide “neutrino-like” data for event reconstruction studies. To satisfy
 1057 the requirement, the beam parameters must span a broad range of particle spectrum
 1058 that are expected in the future neutrino experiment. The particle beam composition
 1059 should consist of electrons, muons, and hadron beams that are charge-selected. The
 1060 expected momentum distributions for secondary particles from neutrino interactions are
 1061 shown earlier in Figure 2.1.1. There is a large spread in the momentum distribution with
 1062 most particles peaked near 200 MeV/c. To cover the momentum range of interest, the
 1063 momentum of the test beam should step from 0.1 GeV/c to 10 GeV/c. The maximum
 1064 electron drift time in the TPC is about 3 ms. To minimize pile-up in the TPC, the
 1065 desired beam rate should be around 200 Hz with the maximum rate below 300 Hz. The
 1066 single-phase TPC consists of two drift volumes. It is desirable to aim the particle beam
 1067 so that the hadronic showers are mostly contained in the same drift volume. However,
 1068 we also plan to take some data with hadronic shower crossing the midplane of the TPC
 1069 from one drift volume to another. The two beam entry angles and positions with respect
 1070 to the LAr cryostat are shown in Figures 19 and 20. The beam nominally enters the
 1071 cryostat slightly downward at an angle of about 6 degrees. Along the horizontal plane,
 1072 the beam enters the cryostat with an angle of 10 degrees. Another possible orientation

1073 (not shown in the Figures) to study APA crossers is to reverse the angle of the beam
1074 instead of shifting the beam parallel to the primary orientation. The summary of the
1075 beam requirements are shown in Table 8.

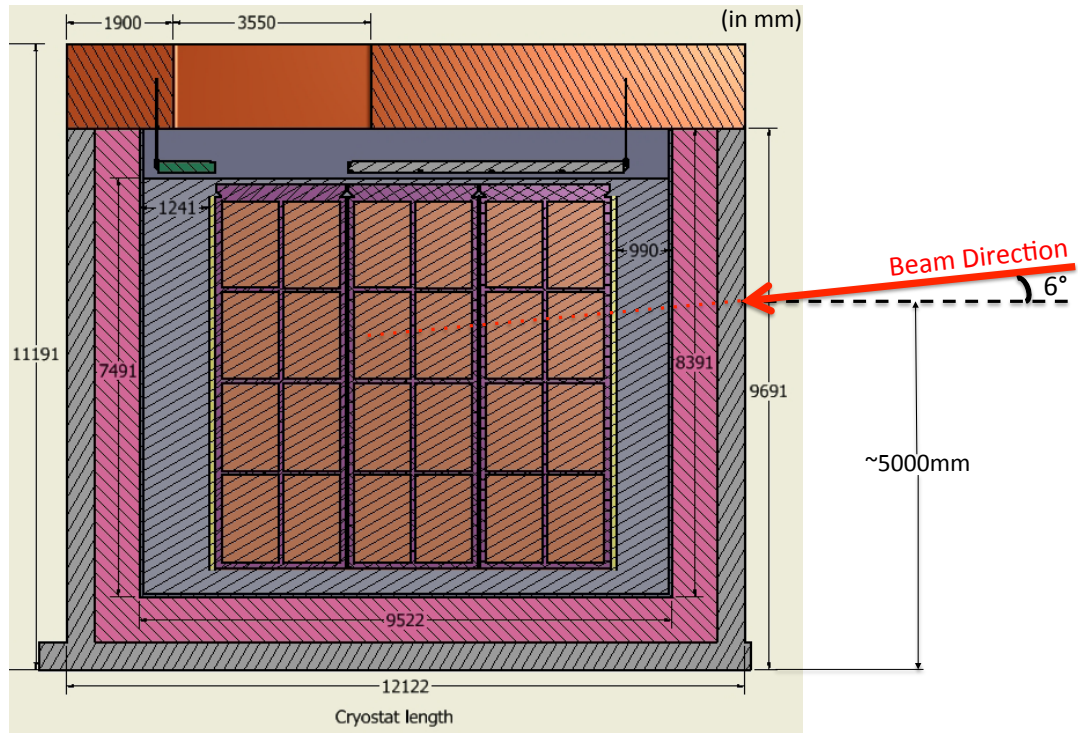


Figure 19: Side view: beam enters the cryostat slightly downward with a dip angle of 6 degrees.

1076 5.2 EHN1 H4ext Beamline

1077 The H4ext is an extension of the existing H4 beamline in Experimental Hall North 1
1078 (EHN1). To produce particles in the momentum range of interest, 60 - 80 GeV/c pion
1079 beam from the T2 target is used to generate tertiary beams. The tertiary particles are
1080 momentum and charge-selected and transported down H4ext beamline to the experi-
1081 mental area. A preliminary layout of the H4ext beamline is shown in Figure 21.

1082 5.2.1 Beam Optics

1083 [Waiting for inputs from Ilias]

1084 5.2.2 Expected Rates and Purity

1085 [Waiting for inputs from Ilias]

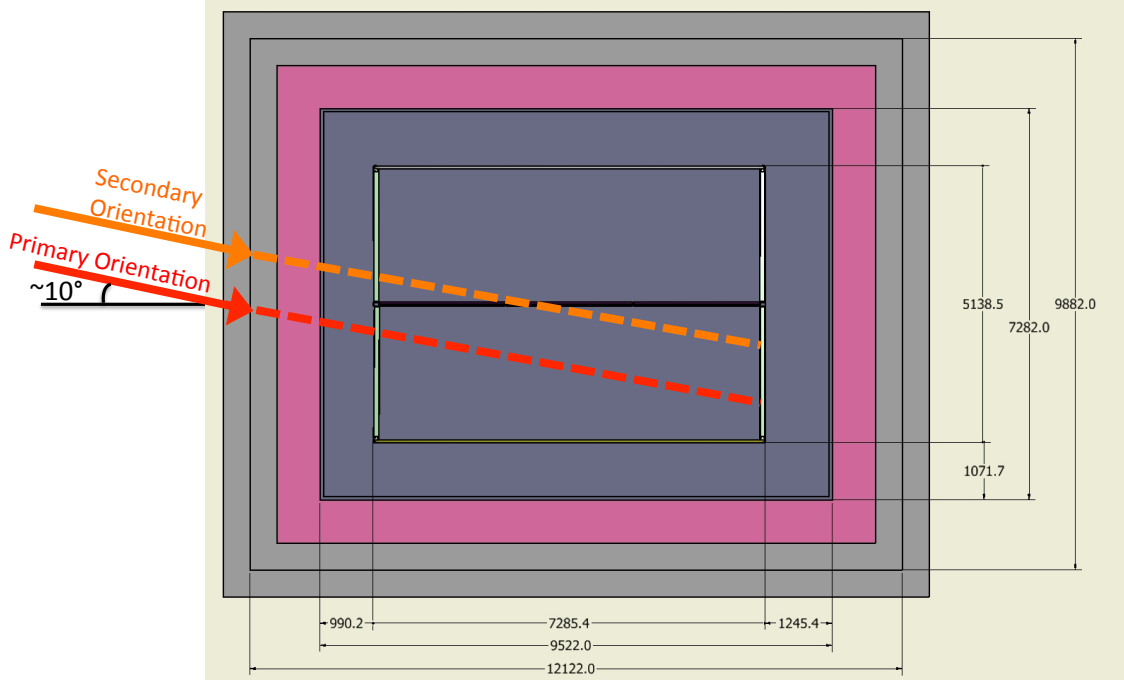


Figure 20: Top view: beam enters the cryostat with an entry angle of about 10 degrees along the horizontal plane. The primary orientation sends the particle beam into one TPC drift volume. The secondary orientation sends the particle beam across the APA.

1086 5.3 Beam Instrumentation

1087 Beam instrumentation provides important information about the characteristics of the
1088 beam. It is expected that a series of detectors will be installed along the beam line to
1089 measure the particle momentum, identify particle type, and track the particle trajectory.

1090 5.3.1 Beam Position Detector

1091 The beam position detector measures the positions of the particle as it traverses the
1092 detector. Two detector technologies are under considerations: wire chambers and scin-
1093 tillating fiber trackers. For the nominal setup, one beam position detector is installed
1094 upstream and another one downstream of the last bending magnet. This pair provides
1095 additional momentum information about the particles as well as the first set of posi-
1096 tion measurements. A third detector is placed right in front of the beam window on
1097 the cryostat wall to provide the last position information before the beam enters the
1098 cryostat.

1099 5.3.2 Particle Identification

1100 In order to have good particle identification over large momentum range, two indepent
1101 particle identification systems are needed in the beamline. The Time-of-Flight system
1102 will be used to cover lower momentum range while a Threshold Cherenkov detector will
1103 be tuned for higher momentum particles.

Table 8: Particle beam requirements.

| Parameter | Requirements | Notes |
|------------------------------------|------------------------------------|--|
| Particle Types | e^\pm, μ^\pm, π^\pm | |
| Momentum Range | 0.1 - 10 GeV/c | |
| Momentum Spread | $\Delta p/p < 5\%$ | |
| Transverse Beam Size | RMS(x,y) < 2.5 cm | At the entrance face of the LAr cryostat |
| Beam Divergence | | |
| Beam Angle (horizontal plane) | $\approx 10^\circ$ | |
| Beam Dip Angle (vertical plane) | -6° (nominal); $\pm 5^\circ$ range | |
| Beam Entrance Position | | |
| Rates | 200 Hz (average); 300 Hz (maximum) | |

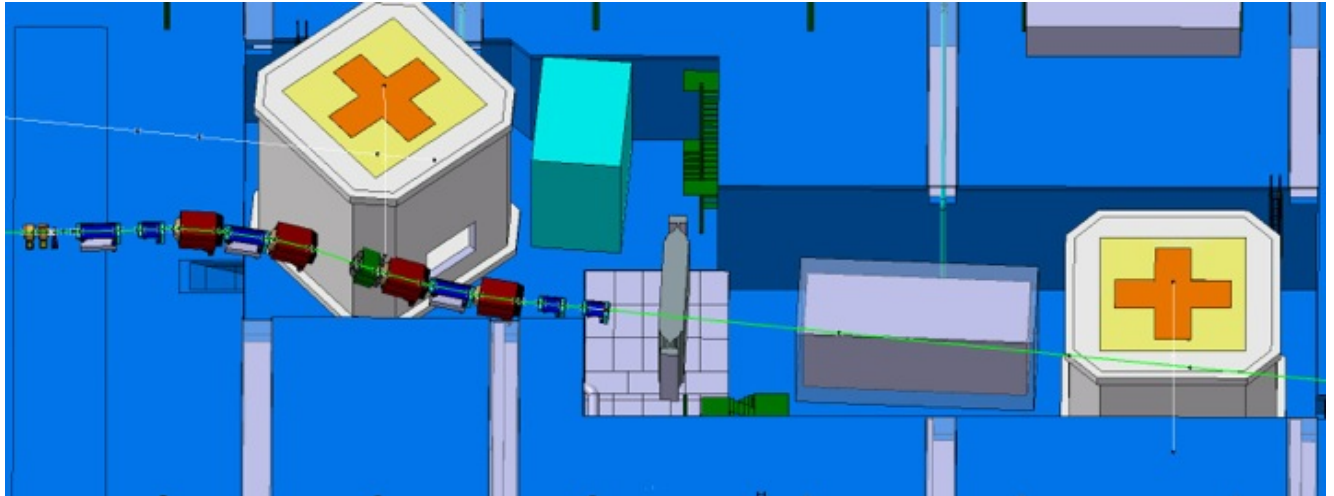


Figure 21: A conceptual layout of the H4ext beamline

¹¹⁰⁴ 5.3.3 Muon Beam Halo Counters

¹¹⁰⁵ The halo counter is a set of plastic scintillator paddles surrounding the beamline. The
¹¹⁰⁶ main purpose is to tag particles (primarily muons from the upstream production target)
¹¹⁰⁷ that are outside of the beam axis, but may potentially enter the TPC volume. The
¹¹⁰⁸ counter information is used to either veto or simply flag these class of events.

¹¹⁰⁹ 5.4 Beam Window on LAr Cryostat

¹¹¹⁰ This section could be absorbed into the cryostat chapter.

1111 6 Computing requirements, data handling and soft- 1112 ware [\sim 3 pages; Maxim/Craig]

1113 The proposed “Full Scale” test of a single-phase Liquid Argon TPC at CERN will build
1114 upon the technology and expertise developed in the process of design and operation of
1115 its smaller predecessor, the 35t detector at FNAL. This includes elements of front-end
1116 electronics, data acquisition, run controls and related systems. We also expect that for
1117 the most part, Monte Carlo studies necessary to support this program will be conducted
1118 utilizing software evolved from tools currently used (2015).

1119 In the test-beam setup, the detector performance will be characterized for different
1120 types of particles, e.g. p , π^\pm , μ^\pm etc (see 2.1). Current plans call for measurements
1121 in pre-defined bins of the incident particle momentum, which will have widths ranging
1122 from tens to hunderds of MeV (see 6.1.3). The volume of data to be recorded shall be
1123 determined by the number of events to be collected in each measurement, such that is
1124 provides adequately low statistical uncertainty of the parameters measured.

1125 In our view, it is optimal to first stage the “precious” data collected from the proto-
1126 type on disk at CERN and then sink it to tape (also at CERN), while simultaneously
1127 performing replication to data centers in the US. For the latter, FNAL is the prime
1128 candidate, with additional data centers at Brookhaven National Laboratory and the
1129 NERSC facility as useful additional locations for better redundancy and more efficient
1130 access to the data from greater number of locations.

1131 6.1 Collecting and Storing Raw Data

1132 6.1.1 Considerations for Event Size Estimates

1133 To set the scale, let’s consider an approximate **upper limit** on the number of channels
1134 with signals above the threshold of zero-suppression, for a single track. For this we
1135 assume digitization rate fixed at 2MHz, and 4312 samples per drift window. In a single
1136 anode plane assembly (APA), it will be approximately of the order of channel count
1137 in the APA, i.e. around 2500, *when the track is parallel to the APA plane*. Since each
1138 sample is 16 bit (or 12 bit in more design), we arrive to the limit of approximately 20MB
1139 per single charged track. For this class of events, the amount of data will scale roughly
1140 linearly with the length of the track, i.e. in cases when a track is stopped or leaves
1141 the sensitive volume there will be less data. Further, in most cases the data will be
1142 zero-suppressed by the front-end electronics (e.g. signals below a certain threshold will
1143 not be included into the outgoing data stream). The exact data reduction factor will
1144 depend on a variety of factors (cf. threshold), but as a rule of thumb it’s an order of
1145 magnitude. *We conclude therefore the events will typically be a few megabytes in size.*
1146 This in fact is supported by previous Monte Carlo studies performed for earlier versions
1147 of LBNE LAr TPC (more detail will be presented below).

1148 At the time of writing, work is being done on the physical design of the Liquid Argon
1149 prototype, and the number of the Anode Plane Assemblies (APA) to be installed in the
1150 detector is not yet finalized. It will likely be 2 or 3, however there is a possibility of this
1151 number to be as high as 6. There is therefore a factor of two or three uncertainty in the
1152 number of readout channels in the detector (e.g. 7680 with 3 APA vs 15360 with 6).

1153 This would affect the amount of data produced by DAQ, although not necessarily by
1154 a factor of two since a large part of the raw data will be zero-suppressed and occupancy
1155 in general is expected to be low. With each additional APA, the number of background
1156 tracks (or track segments) produced by cosmic ray muons will scale very approximately
1157 at a rate of $O(1)$ per APA. Because of the direction of incidence of these tracks and
1158 the fact that in most cases they will be crossing only part of the active volume, we will
1159 account for this by adding data equivalent to approx. 5 extra tracks to each event. This
1160 will very roughly correspond to the upper limit of 6 APAs in the apparatus and thus the
1161 estimate will be conservative.

1162 In addition to the principal sensitive volume where Liquid Argon will serve as active
1163 medium for the TPC, the prototype will also contain a Photon Detector designed to
1164 record light pulses produced in Argon due to scintillation caused by ionizing radiation.
1165 In any realistic scenario, the amount of data to be produced by the Photon Detector will
1166 be quite small compared to that of the Liquid Argon TPC. Same goes for other elements
1167 of the experimental apparatus (hodoscopes, trigger systems etc) and as a result, for the
1168 purposes of this section, we shall focus only on the Liquid Argon TPC as the critical
1169 source of data.

1170 **6.1.2 “Before” and “After” Readout Windows**

1171 As we just mentioned, the detector will be sensitive to background tracks due to cosmic
1172 ray particles. These must be properly identified and accounted for, in order to ensure
1173 high quality of the measurements and subsequent detector characterization. Since over-
1174 lay of cosmic ray muons over beam events is stochastic in nature, the optimal way to
1175 achieve this is by recording signals which were produced “just before” and “just after”
1176 the arrival of the test particle from the beamline. This will enable us to reconstruct
1177 either partial or complete background tracks present in the “main” event.

1178 To ensure complete collection of charge due to such tracks, the additional readout
1179 windows before and after the beam event should equal the nominal total drift time for
1180 the collection volume (approx. 2.1ms). This will triple the amount of data due to cosmic
1181 rays, collected from the detector.

1182 **6.1.3 Statistics and the Volume of Data**

1183 Experimental program for the test includes triggering on a few types of particles over
1184 a range of momenta (see 2.1). We introduce bins for the particle momenta as shown in
1185 the table below. The estimated event sizes listed in the table are based on interpolation
1186 of results from Monte Carlo studies performed earlier for the 10kt version of the LBNE
1187 Far Detector and must be considered as approximate, ballpark estimates. Hadronic and
1188 electromagnetic showers were included in the MC samples so their effect is accounted
1189 for. As a concrete example, for an incident electron of 4GeV/c momentum calculations
1190 indicate an average event size of \sim 2MB, after zero-suppression.

| Particle Type | Momentum Range (GeV/c) | Bin (MeV/c) | Approx. event size, MB |
|-----------------|------------------------|-------------|------------------------|
| p | 0.1-2.0 | 100 | 1 |
| p | 2.0-10.0 | 200 | 5 |
| μ^\pm | 0.1-1.0 | 50 | 1 |
| μ^\pm | 1.0-10.0 | 200 | 5 |
| e^\pm | 0.1-2.0 | 100 | 1 |
| e^\pm | 2.0-10.0 | 200 | 4 |
| K^+ | 0.1-1.0 | 100 | 1 |
| $\gamma(\pi^0)$ | 0.1-2.0 | 100 | 1 |
| $\gamma(\pi^0)$ | 2.0-5.0 | 200 | 5 |

1191 Preliminary plans call for statistics of the order of $10^4 - 10^5$ events to be collected in
 1192 each bin. Depending on the assumptions, this translates into ~ 20 million events total
 1193 (for all event classes) to ensure enough statistics for subsequent analysis. Taking into
 1194 account the cosmic ray overlay and additional readout windows as explained in 6.1.2,
 1195 we arrive to a number of $\sim 1\text{PB}$ for total storage space necessary to host **the raw data**.
 1196 This needs to be looked at as the basis for tape budget. As explained below, this volume
 1197 of data needs to be replicated for assured preservation, in at least one more additional
 1198 facility, hence in effect this number must be doubled when budgeting tape.

1200 6.1.4 Summary of the Data Volume Estimates

1201 The total amount of data to be collected during the prototype operation will be con-
 1202 siderable under all assumptions and estimates. To fulfill the mission of this test beam
 1203 experiment, we expect that we will need tape storage of $O(PB)$ size, and a more modest
 1204 disk space for raw data staging at CERN, for replication purposes. We envisage storing
 1205 the primary copy of raw data at CERN, with replicas at additional locations. There will
 1206 be additional requirements for processed and Monte Carlo data placement.

1207 6.1.5 Raw Data Transmission and Distribution

1208 Moving data to remote locations outside of CERN is subject to a number of requirements
 1209 that include:

- 1210 • automation
- 1211 • monitoring
- 1212 • error checking and recovery (redundant checks to ensure the “precious” data was
 1213 successfully sunk to mass storage at the endpoint)
- 1214 • compatibility with lower-level protocols that are widespread, well understood and
 1215 maintained (cf. gridFTP)

1216 There are a number of systems that can satisfy these requirements, and one of them
 1217 where we possess sufficient expertise and experience is Spade, first used in IceCube [1]
 1218 and then enhanced and successfully utilized in Daya Bay experiment [2].

1219 **6.2 Databases**

1220 A few types of databases will be required for the test:

- 1221 • Run Log, Conditions and Slow Controls records
1222 • Offline Calibrations

1223 Database servers listed in the former item will need to be local to the experiment
1224 (i.e. at CERN) in order to reduce latency, improve reliability, reduce downtime due to
1225 network outages etc. A replication mechanism will need to be put in place the data is
1226 readily available at the US and other sites. The volume of data stored in these databases
1227 will likely to be quite modest.

1228 **6.3 A note on Simulation and Reconstruction Software**

1229 Research effort connected to the “Full Scale” prototype at CERN will benefit from
1230 utilizing simulation toolkits, and tracking and other reconstruction algorithms created
1231 by communities such as former LBNE, and especially during the 35t test at FNAL.

1232 *In order to leverage this software and expertise, appropriate manpower will need to
1233 be allocated in order to create and maintain physics analysis tools necessary to fulfill the
1234 research goals of this experiment.* Given the widely distributed nature of the Collaboration
1235 and the need to use geographically dispersed resources (see 6.4.1, the software
1236 components of these tools will need to be portable, well maintained and validated. To
1237 ensure that this happens, we plan to establish close cooperation among participating
1238 laboratories and other research institutions.

1239 **6.4 Distributed Computing, Workload and Workflow Management**

1241 **6.4.1 Distributed Processing**

1242 At the time of writing, FNAL provides the bulk of computational power for LBNE (not
1243 to mention a few other IF experiments), via Fermigrid and other facilities. We plan to
1244 leverage these resources to process the data coming from the test.

1245 Given the relatively limited amount of beam time for this test, one of the principal
1246 goals will be quick validation of the data collected in each measurement, in order to be
1247 able to make adjustments during the run as necessary. This is a common practice in
1248 other experiment which have ”express streams” to assess data quality (cf. [3]).

1249 There are currently very large uncertainties regarding what scale of CPU power will
1250 be required to process the data, given that tracking, reconstruction and other algorithms
1251 are in a fairly early stage of development. The estimates we have at this point range
1252 from 10 to 100 seconds required by a typical CPU to reconstruct a single event. This
1253 means that utilizing a few thousand cores through Grid facilities, it will be possible to
1254 ensure timely processing of these data.

1255 To ensure adequate capacity, we envisage a distributed computing model where Grid
1256 resources are utilized in addition to FNAL. As an example, we have had good experience
1257 working with the Open Science Grid Consortium.

1258 **6.4.2 Scale of the Processed Data**

1259 As discussed above, we estimate the volume of raw data to be in the petabyte range. We
1260 also must address the offline data, which can be classified as follows:

- 1261 • Monte Carlo data, which will contain multiple event samples to cover various event
1262 types and other conditions during the measurements with the prototype detector
- 1263 • Data derived from Monte Carlo events, and produced with a variety of tracking
1264 and pattern recognition algorithms in order to create a basis for the detector
1265 characterization
- 1266 • Intermediate calibration files, derived from calibration data
- 1267 • Processed experimental data, which will likely exist in a few branches correspond-
1268 ing to a few reconstruction algorithms being applied, with the purpose of their
1269 evaluation

1270 In the latter, there will likely be more than one processing step, thus multiplying
1271 data volume. There is sometimes a question about how much of the raw data should be
1272 preserved in the processed data streams. Given a relatively large volume of raw data, the
1273 answer in this case will likely be “none” - for practical reasons, meaning that the derived
1274 data will be just that, and that the size of the processed data will likely be significantly
1275 smaller than the input (the raw data). Given consideration presented above, we will
1276 plan for \sim 1PB of tape storage to keep the processed data. For efficient processing, disk
1277 storage will be necessary to stage a considerable portion of both raw data (inputs) and
1278 one or a few steps in processing (outputs).

1279 Extrapolating from our previous experience running Monte Carlo for the former
1280 LBNE Far Detector, we estimate that we’ll need a few hundred TB of continuously
1281 available disk space. In summary, we request 2PB of disk storage at FNAL to ensure
1282 optimal data availability and processing efficiency. Access to distributed data is discussed
1283 below.

1284 **6.4.3 Distributed Data**

1285 We foresee that data analysis (both experimental data and Monte Carlo) will be per-
1286 formed by collaborators residing in many institutions and geographically dispersed. In
1287 our estimate above, we mostly outlined storage space requirements for major data
1288 centers like CERN and FNAL. When it comes to making these data available to the
1289 researchers, we will utilize a combination of the following:

- 1290 • Managed replication of data in bulk, performed with tools like Spade discussed
1291 above. Copies will be made according to wishes and capabilities of participating
1292 institutions.
- 1293 • Network-centric federated storage, based on XRootD. This allows for agile, just-
1294 in-time delivery of data to worker nodes and workstations over the network. This
1295 technology has been evolving rapidly in the past few years, and solutions have been
1296 found to mitigate performance penalty due to remote data access, by implementing
1297 caching and other techniques.

1298 In order to act on the latter item, we plan to implement a global XRootD redirector,
1299 which will make it possible to transparently access data from anywhere. A concrete
1300 technical feature of storage at FNAL is that there is a dCache network running at this
1301 facility, with substantial capacity which can be leveraged for the needs of the CERN
1302 prototype analysis. This dCache instance is equipped with a XRootD “door” which
1303 makes it accessible to outside world, subject to proper configuration, authentication and
1304 authorization.

1305 As already mentioned, we plan to host copies of a significant portion of raw and derived
1306 data at NERSC and also at Brookhaven National Laboratory. These two institutions have
1307 substantial expertise in the field of data handling and processing at scale and will serve as “hubs” for data archival and distribution.

1309 **7 CERN neutrino platform test environment [5 pages; 1310 David/Jack/Cheng-Ju/Thomas]**

1311 Description of Requirements, layout and constraints

1312 We propose that the cryostat be housed in the extension of the EHN1 Bat 887 at
1313 CERN, where the cryogenic system components will also be located. (moved to sec 7)

- 1314 • short description of location and orientation of cryostat + cryogenics system in
1315 EHN1 (David)
- 1316 • description of beam line layout (Cheng-Ju)
- 1317 • space for staging, control room, electronics racks, clean room, scaffolding, etc.
1318 (Jack)
- 1319 • power requirements and cooling (Jack ?)
- 1320 • ...

1321 **8 Schedule, organization and cost estimate [~5 pages; 1322 Thomas/Greg]**

1323 **8.1 Schedule**

1324 The schedule of the proposed CERN prototype detector and beam test is dictated by
1325 the ELBNF overall schedule which foresees to place the first 10 kton detector module
1326 underground as early as calendar year 2021. Additional detector modules are expected to
1327 follow shortly thereafter. Ideally information and results from the CERN beam test will
1328 inform the decision about the final ELBNF detector design and hence should be available
1329 as soon as realistically possible. In addition, the LHC long shutdown, which is presently
1330 scheduled for mid-2018 represents a significant constraint on the schedule. In order
1331 to meet the first requirement, data taking for the initial measurement program should
1332 be complete prior to the long LHC shutdown in mid-2018. Figure 22 shows a schedule

¹³³³ which meets this requirement. The shown schedule is based on experience of designing
¹³³⁴ and manufacturing components for the 35t detector which will be commissioned starting
in June 2015 at Fermilab.

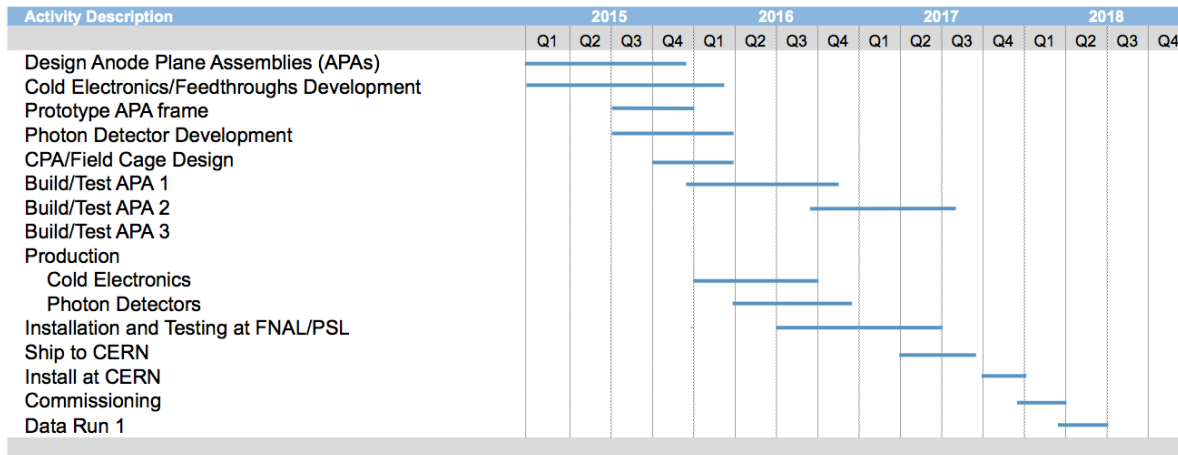


Figure 22: Rolled up version of a draft schedule for manufacturing, installing and commissioning the CERN prototype detector. A 2 - 3 months data taking period is included in the schedule.

¹³³⁵

¹³³⁶ 8.2 Organization

- ¹³³⁷ • working group structure and distributions of tasks/responsibilities

¹³³⁸ 8.3 Division of Responsibilities

¹³³⁹ 8.3.1 Shared responsibilities

¹³⁴⁰ The engineering design of the cryostat and the cryogenics system is considered to be a
¹³⁴¹ shared responsibility between ELBNF and CERN.

¹³⁴² 8.3.2 ELBNF responsibilities

¹³⁴³ The following detector components are expected to be covered by ELBNF project:

- ¹³⁴⁴ 1. XX APAs
- ¹³⁴⁵ 2. CPA
- ¹³⁴⁶ 3. field cage
- ¹³⁴⁷ 4. cold electronics
- ¹³⁴⁸ 5. DAQ hardware and software
- ¹³⁴⁹ 6. ...

1350 **8.3.3 CERN responsibilities**

1351 **The beam line** design, setup of the beam line and beam monitoring instrumentation
1352 are expected to be provided by CERN.

1353 **The cryostat and cryogenics system** are expected to be organized and paid for
1354 by the CERN nu-platform. The scope of the EHN1 cryostat subsystem includes the
1355 design, procurement, fabrication, testing, delivery and oversight of a cryostat to contain
1356 the liquid argon and the TPC.

1357
1358 The following items (incomplete list !) require further discussion. The responsibilities
1359 should be clearly spelled out.

- 1360 • plans for data analysis and publications
1361 • describe overlap/commonalities with WA105 data analysis

1362 **9 Summary [~2 pages; Thomas/Greg]**

1363 this is the summary section

1364 **References**

1365 [1] IceCube Data Movement [https://icecube.wisc.edu/science/data/
1366 datamovement](https://icecube.wisc.edu/science/data/datamovement).

1367 [2] Data processing and storage in the Daya Bay Reactor Antineutrino Experiment
1368 <http://arxiv.org/pdf/1501.06969.pdf>.

1369 [3] Prompt reconstruction of LHC collision data with the ATLAS reconstruction soft-
1370 ware, N.Barlow et al, *Journal of Physics: Conference Series* 331 (2011) 032004

1371 → total estimated page count: ~60 pages